A Bachelor's thesis in Science in Engineering,
Medicine and Technology

Removal of Ultra-Fast MR-gradient and Ballistocardiogram Artifacts in High-Density EEG Data to Detect Sleep

Anders Stevnhoved Olsen
Student ID: s154043

Supervisors:
Morten Mørup, DTU Compute
Sebastian C. Holst, NRU
Claus Svarer, NRU

Handed in May 28, 2018

Technical University of Denmark

Neurobiology Research Unit
Rigshospitalet
Copenhagen University Hospital

1 Abstract

Sleep is believed to be a physiological process critical to the existence of human life. However, despite its seemingly high importance, we know little of what causes, or what is caused by, sleep. A research team at Neurobiology Research Unit (NRU), Rigshospitalet, is set to investigate several aspects of sleep using simultaneous Electroencephalography (EEG) and Functional Magnetic Resonance Imaging (fMRI).

EEG measures electrical activities in the cortex of the brain using electrodes on the scalp, and is well established as the preferred method of sleep observation. It is limited in its spatial characteristics but provides researchers with a tool with high temporal resolution. On the contrary, fMRI can provide functional images of the brain and thus has superior spatial characteristics. The combination of EEG and fMRI gives researchers an opportunity to exploit strengths of two modalities.

The major drawback in using this multimodality setup is the presence of artifacts in the EEG-signal. The Gradient Artifact (GA) is a high amplitude spike with amplitude more than 100 times what is normally seen in EEG. It is caused by the switching of magnetic gradients of the MR-scanner, i.e. when an image is taken. The Ballistocardiogram (BCG) originates from the heart beat and is an artifact heavily amplified by the presence of the strong constant magnetic field of the MR-scanner. Both of these artifacts corrupt the signal enough to disrupt the sleep characteristics of EEG-signals.

Two methods are tested for the removal of GAs: Average Artifact Subtraction (AAS) (Allen, Josephs, and Turner 2000) and Optimal Basis Sets (Niazy et al. 2005). AAS is based on creating and subtracting a template artifact for each EEG channel using a moving average procedure. OBS is an extension of AAS that uses Principal Component Analysis (PCA) to lessen residual artifacts after template subtraction. It is found that, for GA-correction, the two methods are not different.

Three methods are tested for the removal of BCGs: AAS, OBS and Independent Component Analysis (ICA) (Makeig et al. 1996). ICA is an algorithm that decomposes a multivariate signal into statistically independent components. The idea is that heart beat contributions will be captured in one or more independent components. An extension is proposed to ICA that automatically chooses and removes components that carry these BCG contributions. Statistical comparisons are made between the three methods and it is found that they are, in fact, significantly different. Further studies have to be made to determine which method is superior in removing BCGs.

2 Preface

Medicine and Technology is a Bachelor of Science in engineering offered in collaboration between the Technical University of Denmark (DTU) and the Faculty of Health at the University of Copenhagen (UCPH). It is an interdisciplinary education that combines engineering sciences and the biology of the human body.

In the fall of 2017 I enrolled myself in the course Introduction to Machine Learning and Data Mining as an elective course at DTU. I found the subject of advanced data analysis and pattern recognition schemes exciting. As a result, I contacted the course responsible and main lecturer, associate professor Morten Mørup at DTU Compute, to hear of possible opportunities of conducting my Bachelor project in this field. Morten suggested contacting chief engineer Claus Svarer and postdoctoral researcher Sebastian C. Holst, both at Neurobiology Research Unit (NRU) at Copenhagen University Hospital Rigshospitalet. Sebastian was in the beginning of a sleep study that will investigate why humans need to sleep using combined EEG and fMRI. He needed a student to do a comparison of artifact removal methods in EEG-signals.

The Bachelor project was carried out in collaboration with NRU and DTU Compute. This thesis summarizes the work done in the project.

Morten, Claus and Sebastian all functioned as supervisors of this project and deserve acknowledgement and my deepest gratitude for their invaluable help and guidance during all four months.

3 Acronyms

AAS	Average Artifact Subtraction
AD	Alzheimer's Disease
AP	Action Potential
BCG	Ballistocardiogram
CNS	Central Nervous System
DTU	Technical University of Denmark
ECG	Electrocardiography
EEG	Electroencephalography
EMG	Electromyography
EOG	Electrooculography
EPSP	Excitatory Postsynaptic Potential
fMRI	Functional Magnetic Resonance Imaging
GA	Gradient Artifact
GS	Glymphatic System
ICA	Independent Component Analysis
IPSP	Inhibitory Postsynaptic Potential
kTEO	k-Teager Energy Operator
MREG	Magnetic Resonance Encephalography
MRI	Magnetic Resonance Imaging
MB	Multiband
NaN	Not a Number
NMR	Nuclear Magnetic Resonance
NREM	Non-Rapid Eye Movement
NRU	Neurobiology Research Unit
OBS	Optimal Basis Sets
PCA	Principal Component Analysis
REM	Rapid Eye Movement
RF	Radio Frequency
RFA	Radio Frequency Artifact
SWS	Slow-Wave Sleep
UCPH	University of Copenhagen

4 Symbols

B_0	Constant magnetic field in T
Cl^-	Chloride ion
f_s	Sampling frequency in Hz
Hz	Hertz, or one per second (1/s)
K^+	Potassium ion
kHz	Kilohertz
$k\Omega$	Resistance in Kilo-Ohms
ln	The natural logarithm
MHz	Mega-Hertz
ms	Milliseconds
mV	Millivolts
Na^+	Sodium ion
p	p-value
r	Correlation coefficient
s	Second
T	Tesla
T_r	Repetition time
V	Volts
z	z-score
α	Alpha frequency range in Hz
α	Significance level
β	Beta frequency range in Hz
γ	Gamma frequency range in Hz
γ	Gyromagnetic ratio in MHz/T
δ	Delta frequency range in Hz
θ	Theta frequency range in Hz
μ	Mean value
σ	Standard deviation
ω	Angular frequency in Hz
Ω	Resistance in Ohms

Contents

5 Introduction

On average, humans spend one third of their life asleep. Sleep is a physiological phenomenon that happens almost automatically when one has spent too long time awake. Sleep will, sooner or later, force itself upon the human body. However, we still know very little of the biological process of sleep. We know that sleep is an active biological process that can be divided into 4 separate stages of Rapid Eye Movement (REM) and non-REM (NREM) sleep, each with its own characteristics. During a full night of sleep we move through all stages in a somewhat cyclical process (Watson and Buzsáki 2013). Sleep related problems are associated with a number of diseases, such as Alzheimer's disease (AD) and obesity (Olsson et al. 2018). Sleep is also shaped by lifestyle choices and the physiological consequences of living in a society, where computers and smart phones often affect the amount of sleep we get, are still unknown. The fact that a number of important research questions are still unresolved makes it an interesting area to study.

Recently, a theory has been proposed that describes how brain recovery in rodents is mediated by sleep (Nedergaard 2013). The theory is based on data that describes a macroscopic pathway in the central nervous system (CNS) called the glymphatic system (GS), which facilitates clearance of neuronal waste products. The function of the GS is enhanced by up to 90% during sleep when compared to wakefulness (Xie et al. 2013). The pathway may hold answers to understanding the physiological importance of sleep and may even provide a pathophysiological link between sleep and AD, which is known to involve an accumulation of the proteins Beta-Amyloid and Tau (Bear, Connors, and Paradiso 2007). If the GS hypothesis also holds in humans, perhaps pharmacological agents could be designed in the future to improve the effectiveness of the cleaning mechanisms GS and therefore prevent AD.

The first steps in demonstrating the existence of a human glymphatic system, is to measure a glymphatic flow. This thesis forms part of a larger project at Neurobiology Research Unit (NRU) that will investigate a human GS. Applying novel functional imaging techniques such as Magnetic Resonance Encephalography (MREG) and Multiband (MB), the research team examines test subjects both awake and asleep. The subjects are scanned three times at the same circadian time point, two scans involving sleep deprivation. The aim is that the test subjects fall asleep inside the scanner. In order to measure the level of sleep, Electroencephalography (EEG) electrodes are mounted on the scalp of the subjects. EEG is a well established method in sleep monitoring, and guidelines to decode sleep patterns in EEG date many years back.

The simultaneous use of functional magnetic resonance imaging (fMRI) and EEG is relatively new in brain research. On their own, both modalities have advantages and disadvantages. Historically, non-functional MRI has been praised for its good spatial characteristics and is at the front line of anatomical imaging. Conventional MRI measures density of hydrogen atoms and thus can separate different types of tissue. The use of the modality for functional measurements derive from the assumption that more blood flows to areas of the brain that are activated. MRI sequences have been developed to measure this cerebral blood flow. There is a drawback to the use of fMRI for functional measurements, however, and that is its relatively low temporal resolution.

EEG, on the other hand, has brilliant temporal characteristics in the kHz range. Thus, EEG has the ability to measure electric potentials on the surface of the scalp with high temporal precision. As with fMRI, disadvantages follow advantages, and for EEG it is, in

fact, its poor spatial characteristics.

Following the arguments above, it seems that combining fMRI and EEG for functional measurements would provide functional brain researchers with an ideal tool. However, in spite of the advantages of concurrent fMRI and EEG measurements, there are major limitations in the form of EEG artifacts caused by the MRI-scanner. The two most important artifacts are the gradient artifact (GA) caused by the switching of magnetic gradients on the MR-scanner whenever an image is taken, and the ballistocardiogram (BCG), which is a large magnification of heartbeat artifact on EEG primarily caused by the scanner's constant magnetic field (Allen, Josephs, and Turner 2000).

It is the aim of this bachelor project to remove these two prominent artifacts, GA and BCG, using offline signal processing methods. Three methods will be presented: Average Artifact Subtraction (AAS)(Allen, Josephs, and Turner 2000), Optimal Basis Sets (OBS) (Niazy et al. 2005) and Independent Component Analysis (ICA) (Makeig et al. 1996). The first two methods will be tested to remove the gradient artifact, and all three will be used for the removal of the BCG artifact.

The remainder of this thesis includes a Methods chapter, in which background theory on EEG and sleep is presented, as well as a thorough description of the artifacts treated in this project and the methods used for artifact removal. In the Data chapter, recording procedures are described. The Results chapter shows statistical comparisons of the methods in question and finally, the Discussion chapter presents advantages and challenges with the chosen methods and gives suggestions for further examination.

6 Methods

This chapter will present the historical and neuronal background of EEG recordings and sleep classification that forms the theoretical basis for the EEG analyses performed in this thesis. (Sanei and Chambers 2007), (Mordecai P. Blaustein MD 2012) and (Bear, Connors, and Paradiso 2007) will be used as references. Hereafter, a thorough description to the EEG artifacts in concurrent EEG-fMRI recordings is given as an introduction to a subsequent explanation of the artifact removal methods discussed in this thesis.

6.1 Electroencephalogram

Modern sleep research is largely based on the use of the EEG, which offers real time monitoring of brain signals with high temporal resolution (kHz range). This, among other things, facilitates an objective and temporally precise characterization of e.g. epileptic seizures or sleep. Voltage fluctuations in the brain are measured using electrodes placed on the scalp. The discovery of human EEG-signals was done by Hans Berger (1873-1941), who began studying the human brain using string galvanometers in 1920. His first report describing human EEG-signals was published in 1929. Since then, both recording protocols and diagnostic use of the EEG have been further extended.

6.1.1 Neurons

The human brain (termed the Central Nervous System (CNS) along with the spinal cord) consists mostly of nerve cells (neurons) and their helper cells, the glia. Neurons are the primary signal transmitters in the CNS, and they utilize ion concentration differences to create propagating voltage differences across the cell membrane. Each neuron consists of a cell body (soma) with the nucleus, dendrites and an axon branching into several nerve terminals (see Fig.2a). The axon is coated with a fatty layer of myelin sheaths which improve transmission velocity.

Neurons generally have a resting membrane potential of $-70mV$ mediated by potassium ions (K^+) in the intracellular space and sodium (Na^+) and chloride (Cl^-) ions in the extracellular space. These ionic concentration differences are maintained by energy demanding membrane bound Na^+/K^+-pumps. The membrane potential describes an electrical potential difference between the inside of the cell and the surrounding extracellular fluid. When a stimulus is received in a dendrite, such as an action potential from a neighbouring neuron, either an excitatory postsynaptic potential (EPSP) or an inhibitory postsynaptic potential (IPSP) follows. An EPSP is an influx of sodium ions, and subsequently an increase in membrane potential, whereas an IPSP is an influx of chloride and a decrease in membrane potential. A neuron has many dendrites and is therefore continuously stimulated with both EPSPs and IPSPs from other neurons. The local changes in membrane potential in the dendrites distribute spatially via passive propagation and are collected at the Axon Hillock. Here, an action potential (AP) can be generated if the threshold (around $-50mV$) is reached (see Fig.2b). Passively propagating potentials decrease in amplitude exponentially. Hence, multiple EPSPs are needed to reach threshold. APs are single, all-or-none electrical impulses that are transmitted down the axon to the nerve terminals triggering the release of neurotransmitters into the synaptic cleft. Neurotransmitters then trigger postsynaptic potentials

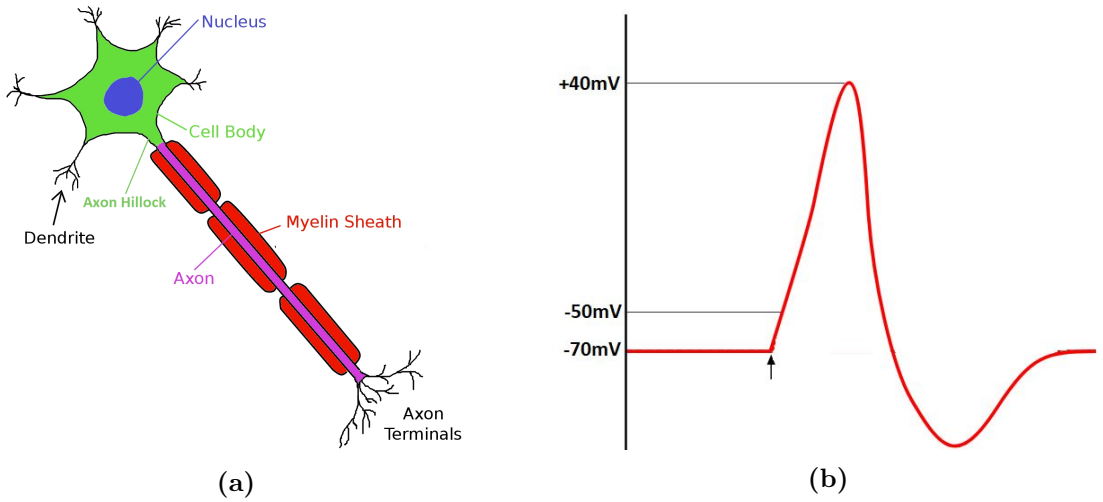

Figure 2: (a): A typical neuron with dendrites, cell body (soma) with nucleus, Axon Hillock and terminal branches. The axon is covered in myelin sheaths maintained by oligodendrocytes (glia) to enhance signal transmission velocity. (b): An action potential starting at the point of stimulus (arrow). Resting membrane potential at about -70mV, threshold at -50mV and peak at +40mV. Both figures are modified from images from Wikimedia Commons.

of dendrites of other neurons. AP propagation is an active process contrary to propagation of postsynaptic potentials, which is a passive process. The upstroke of the AP is caused by an influx of sodium ions that increases with the membrane potential as a positive feedback mechanism until maximum is reached ($+40mV$). This is termed the Nernst potential of sodium. Sodium ion channels inactivate with a delay, paving the way for the downstroke of the AP mediated by a slow efflux of potassium ions. This efflux overshoots a little, creating a small hyperpolarization down to $-80mV$. Finally, the aforementioned Na^+/K^+-pumps restore ion concentrations and membrane potential back to equilibrium (Bear, Connors, and Paradiso 2007). It is worth noting that the precise voltage values are still debated in the scientific community and they should therefore be treated as approximate values.

The postsynaptic potentials caused by the synaptic interaction between cortical neurons generate an electrical field measurable by EEG electrodes. The measurements are summations of graded postsynaptic potentials (either excitatory or inhibitory) from neurons situated perpendicularly to the scalp that act like electrical dipoles pointing from the cell soma to the dendrites (Sanei and Chambers 2007). It is therefore not directly the action potentials that are measured, since these are too short to be measured noninvasively. Instead, it is the slower postsynaptic potentials that are detected. The detected signal is weak since it is attenuated by both the brain, skull and skin. Hence, only larger populations of neurons that are situated along the edge of the cortex can generate large enough electrical potentials to be recorded (Louis and Frey 2016).

6.1.2 Electrodes and their placement

Modern EEG systems consist of a number of delicate electrodes, each with their own differential amplifier. The electrodes are either disposable single-use gelled type, which are

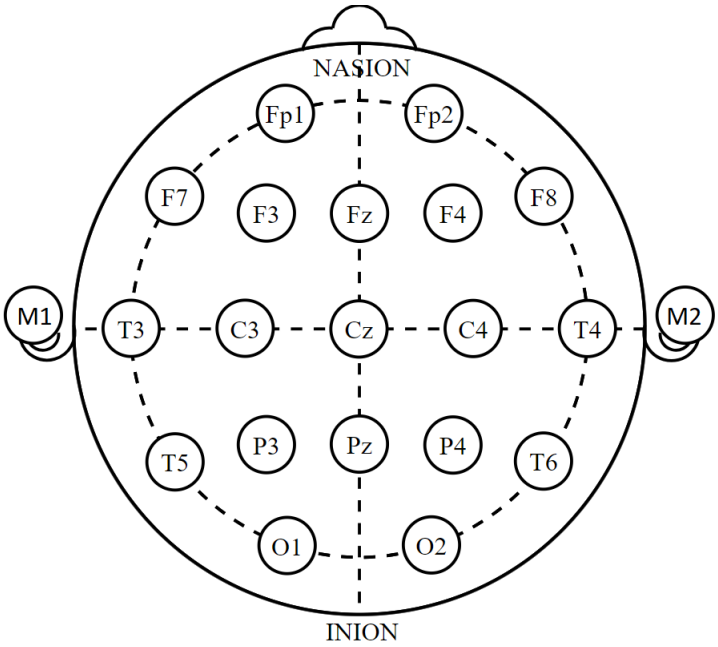

Figure 3: The 10-20 system in Electroencephalography (EEG). Abbreviations are Frontal (F), Central (C), Temporal (T), Parietal (P), Occipital (O) and Mastoid (M). Even numbers are on the right and odd numbers on the left. Figure is modified from an image from Wikimedia Commons.

often used for Electrocardiogram (ECG) measurement, or reusable. The latter can be further subdivided into single electrode caps made of gold, silver or stainless steel and electrode nets, where all electrodes are connected with fabric. The main advantage of using electrode nets is a more precise electrode placement for inter-trial and inter-subject comparison. The downside is that if one electrodes fails, often the whole net has to be replaced. Further, the electrode nets are far more expensive and more uncomfortable to wear when lying down.

For the placement of electrodes on the subject, an international conventional system called the 10-20 system (see Fig.3) has been recognized as the gold standard. This system places 21 recording electrodes and one ground electrode using anatomical landmarks for positioning. When placing electrodes, the EEG specialist finds the Nasion, which is the point between the eyes where the nose "disappears", and the Inion on the back of the scalp and places electrodes here with distances of either 10% or 20% to each other. For more recent systems with up to 256 electrodes, the surplus of electrodes are simply placed equidistantly between the locations shown in Fig.3. For sleep recordings, electrodes around the eyes known as the Electrooculogram (EOG) or electrodes on the chin muscles in the face, known as the Electromyogram (EMG) are added. When the specialist has placed the electrodes he has to make sure the impedance between each electrode and the skin is below a predefined value. If the impedance is too high the noise in the resulting signal may be increased (Kappenman and Luck 2010). Often a maximum impedance of $5k\Omega$ is used.

Because the EEG measures voltage differences, it cannot be measured using only a single electrode. There has to be a reference to a minimum of one other electrode. A differential measurement setup measures the difference in voltage between two electrodes. Depending on

Name	Symbol	Frequency range
delta	δ	$0.5 - 4Hz$
theta	θ	$4 - 8Hz$
alpha	α	$8 - 13Hz$
beta	β	$13 - 30Hz$
gamma	γ	$> 30Hz$

Table 1: List of the conventional sleep rhythms and their frequency ranges.

the goal of the experiment the specialist can choose to measure the difference between two neighbouring electrodes or between an electrode on the scalp and a reference somewhere with minimal EEG and heartbeat detection, such as the mastoid bone behind the ear (M1 and M2 in Fig. 3). Another method is to examine the signal from one electrode with reference to the average of all other electrodes. A channel is data from an electrode with a reference, in this thesis the common reference, which is zero for all time points.

6.1.3 Brain rhythms in general

As previously mentioned, EEG is the primary method of sleep characterization. Specialists are trained to recognize certain rhythms in the fluctuations of the EEG-signal. These rhythms are mainly characterized by their amplitude and frequency. Conventionally, five frequency bands are defined as listed in Tab.1. Delta waves are those of lowest frequency and often also highest amplitude. These are normally associated with deep sleep, but can also appear during wakefulness. Theta waves appear as the subject slips into drowsiness and are seen, for instance, during deep meditation. Alpha waves are typically found over the occipital lobe of the cortex and have been shown to indicate relaxed awareness and lack of attention. Finally, beta waves are those associated with normal wakefulness, active thinking and active attention. Occurrences of Gamma wave frequencies are relatively rare. Multiple articles on the origin of the different brain rhythms have been published in the literature, but a discussion of this is beyond the scope of this text.

6.1.4 Brain rhythms in sleep

Sleep has historically been divided into two arousal states, REM and NREM sleep. NREM sleep is further subdivided into 3 stages. Each NREM stage is associated with its own EEG characteristics, while REM sleep is characterized by eye muscle movement or EOG fluctuations indicating movement of the eyes.

The EEG of a subject slipping from wakefulness to drowsiness indicates absence of myogenic (muscle movement) artifacts as well as loss of normal Alpha rhythm and an increase in Theta waves, as previously mentioned. As the subject reaches NREM stage 2 sleep, special events called K-complexes and sleep spindles are observed. A K-complex is a single, high voltage, broad contoured event whereas sleep spindles are high frequency ($11-15Hz$) medium voltage bursts with a period of one second. NREM sleep stage 3 also goes under the term Slow-Wave Sleep (SWS). Here, waves in the delta frequency band are the most prominent and amplitudes are higher than in the other stages. The state of vigilance during SWS is often called 'deep sleep'. Research has shown that a descent from stage 1 to SWS and a subsequent

ascent to stage 1 happens several times during a full night of sleep. REM sleep is often entered from stage 1 sleep and is the period where dreams are most vivid, hence its pseudonym 'dream sleep' (Watson and Buzsáki 2013). This pseudonym is a common misconception as modern sleep research show dream recall from both NREM and REM sleep.

6.2 EEG artifacts in simultaneous EEG-fMRI measurements

Modern brain diagnosis and research methods are mainly based on the acquirement of high quality and precise signals and images.

As previously mentioned, EEG provides superior temporal resolution (in the range of kHz) compared to medical imaging methods for brain measurement purposes. However, EEG cannot reveal detailed spatial information of the location of neural activity. Thus, one of the largest limitations of EEG is its inability to measure signals originating from deep parts of the brain. Such spatial information could be provided by fMRI and thus the simultaneous use of EEG and fMRI seems straightforward. However, in spite of the many advantages of concurrent EEG and fMRI measurements, there are major limitations in the form of artifacts in the EEG-signal. For further details, see (Eichele et al. 2010).

6.2.1 Magnetic Resonance Imaging

In order to fully understand the cause of EEG artifacts, a short introduction to Magnetic Resonance Imaging (MRI) is in place. See (Hanson 2009) for a more thorough explanation. MRI is an application of Nuclear Magnetic Resonance (NMR), which exploits the fact that some nuclei have magnetic properties. Mainly Hydrogen nuclei (or, single protons) are used for imaging purposes. In the presence of a constant magnetic field, each nucleus spins around itself with an angular frequency ω, called the resonance frequency, determined by the Larmor equation (see Eq.1).

$$\omega = \gamma \cdot B_0 \tag{1}$$

Here, γ is the gyromagnetic ratio, a constant specific to each atom type, and B_0 is the strength of the external magnetic field. As the nucleus spins it creates its own small magnetic field represented by a magnetization vector M, which then, in the presence of an external magnetic field, precesses around B_0. The situation is visualized in Fig.4. The precession of the magnetization vector M around B_0 is far from perfect. However, when imagining the summation of magnetization vectors of billions of Hydrogen nuclei all having a precession slightly skewed towards B_0, it becomes clear that there will be a net magnetization pointing towards the B_0-field.

The magnetic nuclei are then excited by a radio frequency (RF) wave with frequency equal to the left hand side of the Larmor equation. This causes the individual M vectors to be pushed away from the B_0-field. The time it takes for the magnetization to relax to its previous state is measurable and dependent on which molecules the nuclei are part of. For example, Hydrogen is present in both water and fat. In fat, due to the size of the molecule, each Hydrogen nucleus is more "fixed" in place and may relax quicker than a nucleus in water.

In order to distinguish small areas within the body, so called magnetic gradients are used. These are similar to the constant magnetic field B_0 but located perpendicularly (i.e. from

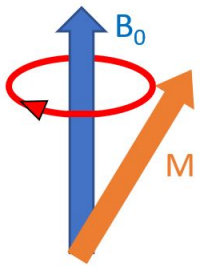

Figure 4: In the presence of a strong magnetic field (B_0), the magnetization vector (M) of some atoms, such as Hydrogen, will precess around B_0.

one ear to the other) and are much lower in strength. The gradients switch on whenever an image is taken, which causes small but precise deviations in the B_0-field within the body. According to the Larmor equation, a deviation in B_0 results in a proportional change in resonance frequency ω.

According to the literature, and following the simplified introduction to MRI above, we can list some probable causes for artifacts in an EEG-signal recorded simultaneously with MRI. These artifacts may be caused by:

1. The excitation of nuclei by very-high frequency radio waves
2. The switching of magnetic gradients
3. The constant magnetic field B_0

Indeed the above listed effects of imaging with MRI do cause artifacts in the EEG-signal, albeit in different ways. The following sections are devoted to an introduction to these artifacts. Artifacts caused by the first two items on the list will be collected in one section devoted to imaging related artifacts and cardiac related artifacts indirectly caused by the B_0-field are presented in the subsequent section.

6.2.2 MRI-imaging related artifacts

There are two types of imaging artifacts to be noticed, the Radio Frequency Artifact (RFA) and the Gradient Artifact (GA). The former is the result of induced RF pulses with a frequency determined by the Larmor equation (Eq.1). For Hydrogen atoms the gyromagnetic ratio is $\gamma = 42.57MHz/T$. However, because this frequency is much higher than the EEG-signal itself it can be removed using analog low-pass filtering with relative ease.

The GA results from the switching of magnetic gradients in the MR scanner, which is necessary for spatial separation of magnetic resonance signals in order to acquire images. The form of the artifact changes according to the imaging sequence being used. Fig.5a shows an example of the GA during 10 seconds of scanning. At first glance the GA completely disrupts the EEG-signal since it consists of steeply rising fast transients with a magnitude of more than 100 times what is normally seen in EEG. The shape of the artifact varies from channel to channel. Within each channel and imaging sequence, however, the artifact shows little fluctuation over time (see Fig.5b) and is therefore of exogenous character. Unlike the RFA, the GA disrupts the signal with a frequency content well within the bandwidth of

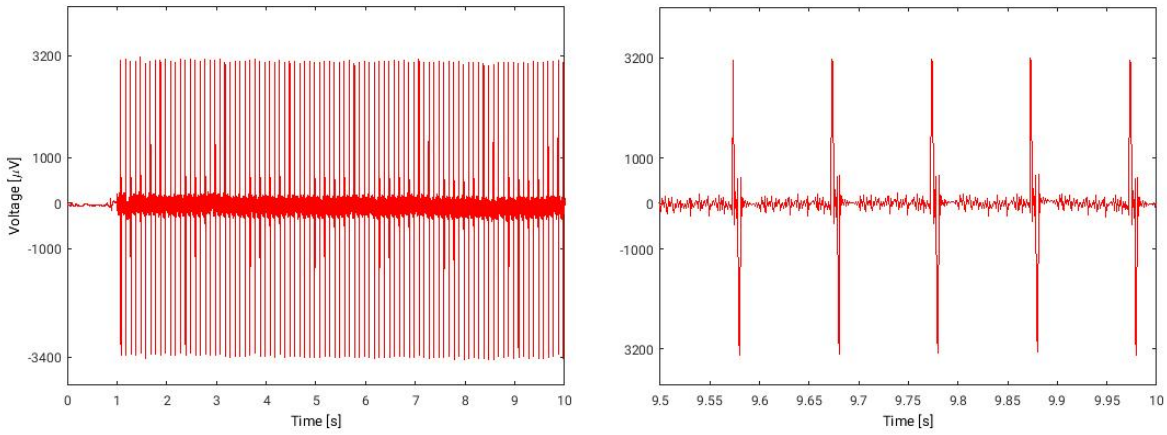

(a) **(b)**

Figure 5: The gradient artifact (GA). (a): 9 seconds of an imaging sequence after 1 second with no imaging. (b): Zoomed in on 0.5 seconds of an imaging sequence.

interest ($< 70Hz$) and cannot be filtered during acquisition efficiently enough to cancel out the artifact. Despite the severity of the GA, the corrupted signal contains the EEG-signal "riding on top" of the GA. This fact renders the statistical removal of the GA feasible (Eichele et al. 2010).

6.2.3 Cardiac related artifacts

The Ballistocardiogram (BCG) is an artifact that is always present on the EEG in the MR-scanner's constant magnetic B_0-field, and is neither dependent of nor changed during image acquisition. The BCG is a fluctuation in the EEG-signal originating from the cardiovascular system (see Fig.6). It is endogenous to the subject yet exogenous since it is induced by the static B_0-field, making it a heterogeneous artifact. The BCG-artifact is time-variant to a higher degree than the GA, meaning that both the shape and scale of the artifact suffers from temporal variations and is not dependent on MR sequence. Likewise, the time from heartbeat to BCG also vary from channel to channel depending on the distance from the heart. The approximate delay is 200ms. The frequency content (about $1Hz$) of the artifact overlaps that of the EEG-measurements. Especially SWS, with frequencies in the delta range and larger amplitudes than observed during e.g. wakefulness, is very similar to the BCG, consequently making it very difficult to recognize deep sleep even in GA-free simultaneous EEG-fMRI recordings. Heartbeat fluctuations in EEG recorded outside the scanner have not been described to the same extent as inside the scanner, making the BCG a simultaneous EEG-fMRI problem only.

The cause of the BCG is still debated in the scientific community. It is believed that the cardiac cycle results in small pulsations in the scalp beneath the electrodes and therefore minor fluctuations in the magnetic field surrounding each electrode. This movement of electrodes and conductive blood-flow inside the magnetic field may induce the artifacts. It has

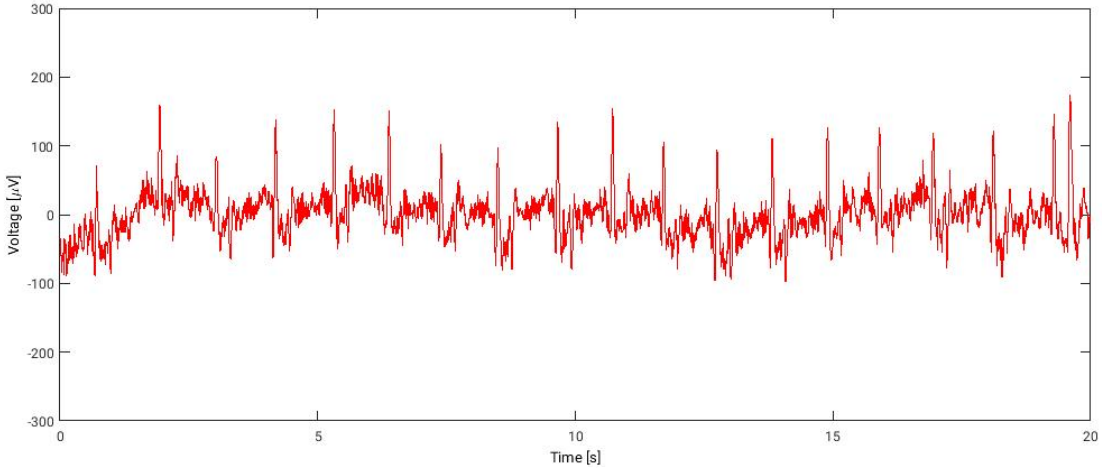

Figure 6: The Ballistocardiogram (BCG) shown clearly in 20 seconds of in-scanner Electroencephalography (EEG) recordings without image acquisition. No digital filtering is applied. Note the different amplitude of the BCG compared to the Gradient Artifact (GA).

been shown that the stronger the B_0-field, the larger the amplitude of BCG (Eichele et al. 2010).

6.2.4 Motion related artifacts

EEG artifacts can also be caused by motion, both inside and outside a static magnetic field. Sudden small voluntary head movements are inevitable and may be more prominent due to the discomfort of lying with the head on top of EEG electrodes in the MRI-scanner. These movements corrupt the signal, more so inside than outside the scanner for the same reasons described above for the BCG. Besides voluntary movements, slow involuntary movements also occur, perhaps linked to respiration or caused by the subject getting to rest inside the scanner. These slow movements are not always directly visible to the naked eye on the EEG-signal but never the less do have an impact on both the GA and the BCG. This problem needs to be taken into account when designing and discussing artifact removal algorithms. Further, movement due to the respiratory cycle is also visible in the GA-free EEG-signal. However, the frequency component of respiration (approx. $0.2Hz$) is lower than the delta frequency band of the EEG, and can therefore be removed with a high-pass filter. Finally, vibrations from the cryogenic pump, which is used to cool the super conducting magnet thereby ensuring a constant magnetic B_0-field, has also been shown to affect the EEG-signal, albeit to a small degree. The same goes for the MRI-scanner ventilation system.

In conclusion, the GA and BCG are the two most important artifacts in simultaneous EEG-fMRI, and neither of them are subject to simple methods of removal such as filtering. The GA and BCG are similar in their repetitiveness, but the GA, being of exogenous character, shows less variability between single artifacts than the BCG as seen in Figs. 5 and 6. Even though it seems that the GA corrupts the underlying physiological signal more than the BCG, both have shown to cause problems when determining sleep stages. The GA and BCG differs to voluntary motion related artifacts in that the latter shows no repetitiveness.

Furthermore, it is very difficult to remove these while preserving the underlying EEG-signal. However, movement artifacts may very well affect the GA- and BCG removal algorithms presented in the next few sections, and therefore must be taken into consideration. However, the focus in this thesis is on the removal of the gradient and ballistocardiographic artifacts.

6.3 Methods of artifact removal

This chapter presents three algorithms described in the literature: Average Artifact Subtraction (AAS)(Allen, Josephs, and Turner 2000), Optimal Basis Sets (OBS)(Niazy et al. 2005) and Independent Component Analysis (ICA)(Makeig et al. 1996). The first two were developed with GA and BCG removal purposes. These are the general methods of choice in simultaneous EEG-fMRI experiments in the literature. The latter was developed before simultaneous data acquisition was proposed and therefore has a more general purpose.

In this project only AAS and OBS will be tested for GA removal. Meanwhile, all three methods will be tested for BCG removal. For the removal of BCG, all methods require a successful detection of heartbeats from an ECG signal. Hence, the first section describes the QRS-detection algorithm chosen for this problem.

6.3.1 QRS-detection

As a prerequisite for successful removal of BCG, a robust QRS-detection algorithm is needed. The one presented here was first introduced by (Christov 2004) and later modified and expanded by (Niazy et al. 2005).

A well known method of separating R-peaks from the rest of an ECG-signal is to square the signal. In this way the difference between large amplitude and low amplitude components becomes larger. The k-Teager Energy Operator (kTEO) is a special non-linear filtering method that elaborates on this line of thinking. It is developed to emphasize specific frequencies in a signal. With regards to peak detection in ECG signals, the objective is to enlarge the R-peak and suppress everything in between.

The kTEO is defined in Eq.2:

$$\mathbf{X}[n] = \mathbf{E}^2[n] - \mathbf{E}[n-k]\mathbf{E}[n+k] \tag{2}$$

where X is the output, a so-called "complex lead", and E is the ECG signal band-pass filtered with cut-off frequencies at $7Hz$ and $40Hz$. The value k is adjusted for each data set according to Eq. 3.

$$k = \frac{f_s}{4f_d} \tag{3}$$

where f_s is the sampling frequency and f_d is the desired frequency to emphasize, in this algorithm set to be the 10th harmonic of the ECG.

An ECG-signal example and its complex lead constructed using the kTEO is shown in Fig.7. Similarly to Fig.6 these data are acquired inside the MR-scanner in a period with no image acquisition. Hence, the gradient artifact does not corrupt this example signal. However, even the ECG signal is subject to ballistocardiographic artifacts. Looking at Fig.7a we do not see the same characteristics as in a normal ECG-pattern with P, Q, R, S and T-peaks. The BCG may very well be the reason for this. Looking at the complex lead (Fig.7b) we see a large scaling on the y-axis and the R-peak is distinguished clearly.

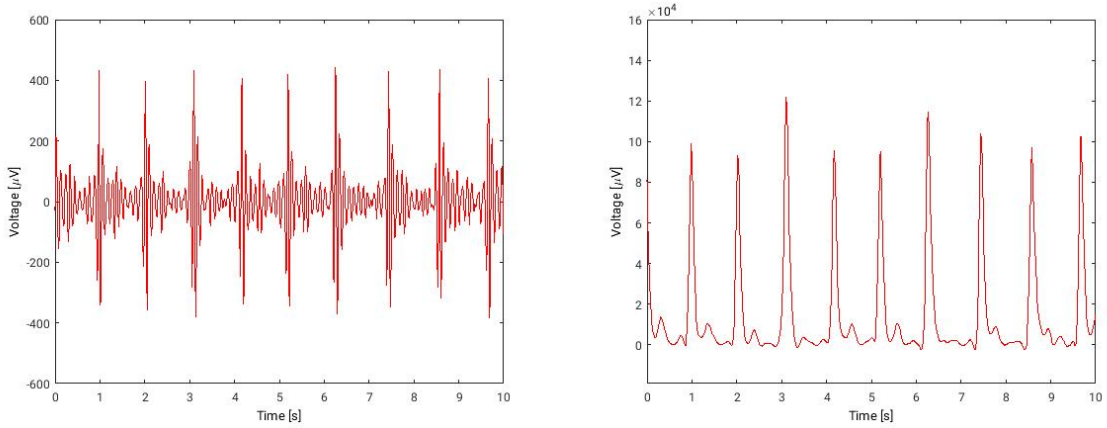

(a) **(b)**

Figure 7: Electrocardiogram (ECG) signal inside the MRI-scanner but without imaging. (a): Raw ECG signal. (b): The complex lead constructed using the k-Teager Energy Operator (kTEO). Notice the difference in scaling on the Voltage axes.

An adaptive threshold technique is then applied to the complex lead. This algorithm combines three different thresholds:

- Steep-slope threshold
- Integrating threshold for high-frequency signal components
- Heartbeat expectation threshold

The steep-slope threshold is the most important of the three. It sets an initial threshold at 60% of the maximum voltage of the first five seconds of the complex lead. 200ms after the threshold has been reached it decreases linearly until the next high peak reaches it. Then, the threshold adapts to 60% of the maximum value of the new peak. This continues for the entire length of the signal and can be performed in real time.

The integrating threshold raises the combined threshold if electromyogram noise accompanies the ECG, such as movement. This method ensures that the R-peak threshold is kept constant during a period of movement, where the R-peak is no longer directly visible. Finally, the heartbeat expectation threshold serves to detect low amplitude R-peaks followed by high amplitude peaks.

The output of the adaptive thresholding algorithm by (Christov 2004) is a vector $\mathbf{P}$ of zeros and ones, where the ones represent a detected peak. The algorithm is expanded by (Niazy et al. 2005) the following way: The vector $\mathbf{P}$ is divided into 20 second sections and in each section, all R-R intervals are calculated. The median and standard deviation of the R-R intervals are then computed. To correct for false positives, a detected peak is removed if the R-R interval from the previous peak falls below the median minus 3 standard deviations. Further, to correct for false negatives, if an R-R interval in a section is larger than 1.5 times the median in this section, a peak is added in $\mathbf{P}$ where missing.

6.3.2 Average Artifact Subtraction

Average Artifact Subtraction (AAS) was originally proposed by (Allen, Josephs, and Turner 2000) and was developed under the assumption on repetitiveness of artifacts. In the algorithm a template artifact is created by using a trigger signal as a time-locking event and then averaging over repeated artifacts. This is done on high-pass filtered data to avoid interruption from e.g. the respiratory cycle. The trigger signal depends on the artifact in question. For the GA, a vector of slice-timings, indicating a switch of gradients, is used as the time-locking event whereas for BCG the detected QRS-complexes is the indicator of artifact. Slow involuntary movements are accounted for by constructing the template artifact using a moving average of a specified number of artifacts. Since the morphology of artifacts differ from channel to channel, the template calculation and subsequent artifact removal is done for each channel separately.

For GA removal, single artifacts that differ from the current mean can be accounted for by only including them in the average template if they are closely correlated to the rest (e.g. inclusion only when the correlation coefficient $r > 0.975$). Because of the high temporal variability of the BCG, it is difficult to specify a threshold coefficient for this artifact. Furthermore, the steep transients of the GA requires a high sampling frequency in order to align the time-locking point precisely and thereby to avoid temporal "jitter". Sampling rates in the kHz range, or an upsampling procedure can be used to circumvent this problem.

For BCG removal using AAS the procedure is similar to GA removal, except that the detected QRS-peaks are shifted forward in time by 210ms to account for the delay from heartbeat to fluctuations in the EEG-signal. However, even though the assumption on similarity between single artifacts may hold true for GA, adjacent cardiac cycles and the morphology of the resulting BCGs may change more.

6.3.3 Optimal Basis Sets

This algorithm was developed as an expansion to AAS to lessen residuals after subtracting a local moving average template artifact (Niazy et al. 2005). Abrupt deviations in neighboring gradient or ballistocardiographic artifacts are not always captured by the AAS algorithm. Only slow involuntary movements are accounted for by the moving average window. For GA removal, OBS combines the local moving average template construction with a combination of basis functions derived from a principal component analysis (PCA) of the cleaned EEG-signal with residuals. PCA is a statistical procedure that converts a data set into a set of uncorrelated variables called principal components. The aim is to remove the residuals, i.e. excess artifacts not captured and removed by the AAS algorithm alone. The algorithm is designed as follows:

1. Similar to AAS, a template artifact is constructed using a moving average window on high-pass filtered data of high sampling rate. This produces a vector $\mathbf{Q}$ of estimated artifacts. $\mathbf{Q}$ is subtracted from the original data to produce the vector $\mathbf{Y}$.

2. The "cleaned" signal with residuals $\mathbf{Y}$ is divided into artifact long segments. These segments are collected in a matrix $\mathbf{S}$ of size $[p, q]$, where p is the number of segments and q is the number of samples in each template.

3. "Demeaning" the matrix **S**. This is done by removing the row-wise mean, which corresponds to removing the mean of each segment. Next the column-wise mean is subtracted, which corresponds to removing the mean of the residuals.

4. PCA is then performed on **S**, and the variations in the residual artifacts will be captured in the principal components of **S**.

5. The first C components constitute an optimal basis set **B**. The data in which the average artifact has been removed (**Y**) can now be described as follows for each segment j:

$$\mathbf{Y}_j^{'} = \mathbf{B}\beta_j + \epsilon_j$$

   Here, β is a vector of weights of length C, ϵ is an error term for the segment.

6. The weights β are then computed for each segment by minimizing the error term.

7. The number of principal components C is chosen according to explained variance. The projection of **S** onto the C principal components, which is now the estimated residual artifact, is then added to **Q** and subtracted from the original data. to produce cleaned EEG-data with less residual artifacts.

8. The procedure is repeated for all channels

Because BCGs have high temporal variability, the OBS approach is designed not to assume any temporal relation between adjacent artifacts. The procedure for BCG removal is the same as for GA removal, except QRS-detection incidents are shifted forward in time by 210ms to account for delay from heartbeat to BCG, similar to using AAS for BCG removal.

6.3.4 Independent Component Analysis

Contrary to the AAS and OBS algorithms described above, the ICA approach will only be tested for the removal of ballistocardiographic artifacts. The technique was originally presented by (Bell and Sejnowski 1995) and first described in use on EEG-signals by (Makeig et al. 1996). For further details on the statistical development of ICA, see (Hastie, Tibshirani, and Friedman 2009).

The key assumption to ICA is that signals recorded from the sensors (EEG channels) are a combination of independent cortical and subcortical activities. The concept is that the EEG-signals can be decomposed into components that represent an activity independent of other activities. These components are spatially fixed to the position of a single electrode but can be spread across a larger area of the scalp. The use of ICA for removing BCG artifacts may enable us to determine the combined cardiac contribution to all electrodes. The aim is that the BCG will be captured as a single independent component that is distributed across all electrodes on the scalp. The component can then be recognized manually and removed from all EEG channels.

Mathematically, ICA is an algorithm that finds a matrix **A** and a matrix **S** so that the elements **S** of $\mathbf{X} = \mathbf{A} \cdot \mathbf{S}$ are statistically independent. The main constraint being that the multivariate probability density function of **S** factorizes, i.e.:

$$f_{\mathbf{S}}(\mathbf{s}) = \prod_{i=1}^{N} f_{S_i}(s_i) \tag{4}$$

The technique of computing **A** and **S** is a whole research area in itself, and is thus out of the scope of this project. However, we can elaborate on the assumptions the algorithm makes to separate independent components in EEG data:

1. The complex EEG dynamics can be modeled using a number of statistically independent brain processes.
2. The propagation delay of electrical activity through the brain is negligible.
3. The number of independent signal sources is the same as the number of sensors.

According to assumption 3, the algorithm can separate N sources, where N is the number of scalp electrodes used in the measurements. However, the assumption that the number of independent signal sources is exactly equal to the number of independent activities is unrealistic, since there are currently no ways of separating and counting independent processes in the brain. Further, we have previously discussed that the time delay from heartbeat to fluctuation in the EEG-signal depends on the distance the blood has to travel through vessels to reach the skin under the electrodes. Thus, assumption 2 is also unrealistic. It is therefore expected that BCG contributions will be distributed in more than one component. These components will then show the BCG with different delays. Because of this, using ICA for BCG removal becomes particular relevant in high-density EEG recordings, since there is a higher probability that BCG artifacts will be captured in components that together cover the entire surface of the brain.

A concern with using ICA for artifact removal is that the algorithm may compute a new set of independent components for each data set, and the amount of those that carry BCG may vary considerably. Thus, comparisons between data sets may prove the algorithm to perform qualitatively different.

6.3.5 Proposed extension to ICA

The main flaw using the technique presented by (Makeig et al. 1996) is that the components (i.e. the output of the algorithm) has to be scrolled through by the researcher, and components containing contributions from BCG has to be recognized manually. Hence, objectivity is lost since it is necessary to subjectively choose components to remove. Further, if the EEG-data is collected with a high-density electrode system, the algorithm computes as many components as EEG-channels. The time spent on selecting components to remove may be reason enough to opt out of using this algorithm.

These drawbacks can be avoided by exploiting the repetitiveness of the components containing BCG compared to those that do not. We therefore propose an extension of the algorithm with the following steps:

1. Every component **C** from the ICA are divided into segments **B** with length comparable to one heartbeat. The length is determined to be the average R-R distance from the QRS-detection algorithm across the entire data set. The segments are separated using the detected R-peaks as time onset.

2. The segments **B** are then averaged. A new vector **V** is created by repeating the averaged segment every time a heartbeat is detected. **V** then has the same length as **C**.

3. The Pearson correlation r between **C** and **V** is computed.

4. The procedure is repeated for all components.

5. Components with a correlation r above a predefined threshold are selected and removed from the data set.

The idea is that independent components capturing BCG artifacts will show a high degree of similarity between adjacent artifacts, and thus a higher correlation coefficient. The extension will be used with ICA in this thesis.

6.4 Data processing work flow

Due to the aforementioned similarity between adjacent single GAs and the fact that trigger signals from the MRI-scanner can be used as time onset for template construction with a high level of precision, the choice to remove GAs before BCG-correction is straight forward. In the Results chapter, statistical comparisons between the two methods of GA-correction are presented first and the three methods of BCG-correction second.

Comparisons between the three methods of BCG-correction will be done on data, where GAs have been removed using AAS. Thus, it is not the combination of GA-removal and BCG-removal methods that are compared. The work flow can be seen in Fig.8. AAS was chosen for GA removal prior to BCG-correction because of its speed compared to OBS. Before the BCG removal step, QRS-detection is performed on GA-free data.

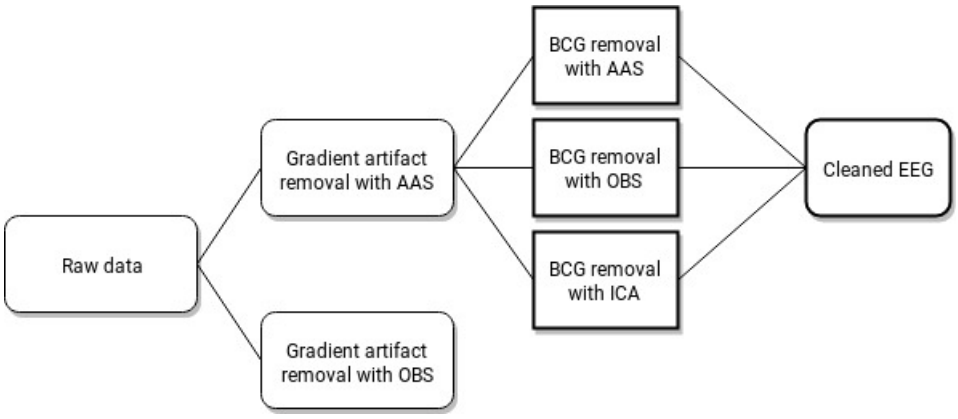

Figure 8: The statistical setup of this thesis. Gradient artifact (GA) removal will be tested using two methods: Average Artifact Subtraction (AAS) and Optimal basis Sets (OBS). Ballistocardiogram (BCG) removal will be tested on data, where GAs have been removed using AAS. The methods for BCG-removal are AAS, OBS and Independent Component Analysis (ICA).

7 Data

This chapter serves to present recording procedures and characteristics of raw data before any of the signal processing described in the Methods chapter is performed. The data were collected prior to the beginning of the project and thus did not involve the author of this thesis. Many test subjects were recruited to be part of a larger project that will investigate a human GS, and only a subset of the recorded data were used in this thesis.

7.1 Recording procedures

Two healthy volunteers were equipped with a Geodesic Sensor Net made by Electrical Geodesics, Inc. comprised of 256 electrodes. Two ECG electrodes were mounted across the heart. EEG and ECG were recorded continuously during fMRI-scanning with a sampling frequency of 1000Hz. The EEG and ECG signals were collected in the same battery powered amplifier in the room of the MR-scanner. Optic cables led the amplified signals from the MR room to a computer outside the MR room where the data were stored as .bin-files. This setup minimizes the 50Hz power line interference that may cause difficulties in experiment setups where EEG equipment is not powered by batteries.

Two fMRI-sequences were used interchangeably: Magnetic Resonance Encephalography (MREG) and Multiband (MB). MREG lasts 296 seconds and MB 301 seconds. MREG has a repetition time (T_r) of $T_r = 0.100$ seconds and thus scans the entire brain of the subject 2961 times per ≈ 5 minute sequence. For Multiband the numbers are $T_r = 0.215$ seconds and 1400 scans in a sequence. Before each MREG sequence the scanner performed a roughly one minute calibration image. Each time an fMRI-scan was performed, i.e. MREG or MB, the MRI-scanner produced a trigger signal that was sent to the same amplifier that the EEG and ECG signals were collected in. Collecting the EEG, ECG and trigger signal in the same amplifier ensures optimal temporal synchronization between the three signals.

7.2 Raw data

Each EEGECG recording typically contains data data from one calibration sequence, an MREG sequence and a MB sequence, all separated by latency periods of approximately 10 seconds. However, EEG recordings during some scans were interrupted in the middle of an imaging sequence and were not saved properly. Only EEG-data from uninterrupted periods of imaging sequences were kept. In total, 7 MREG and 5 MB sequences were collected.

Data was loaded into MATLAB (The MathWorks, Inc.) using a function written by Pierre LeVan, Universitätsklinikum Freiburg, that reads the .bin-files as EEG, ECG and trigger signals. A typical collection of EEG data from a derivation that corresponds to F8 in Fig.3 minus the common reference can be seen in Fig.9. Here we see three imaging sequences: a calibration procedure, MREG and MB. The green areas depict periods where trigger signals were collected from the MRI-scanner indicating a switch of magnetic gradients. It can be seen that there are no trigger signals from the first 3 seconds of MB-imaging as well as in periods of calibration sequences.

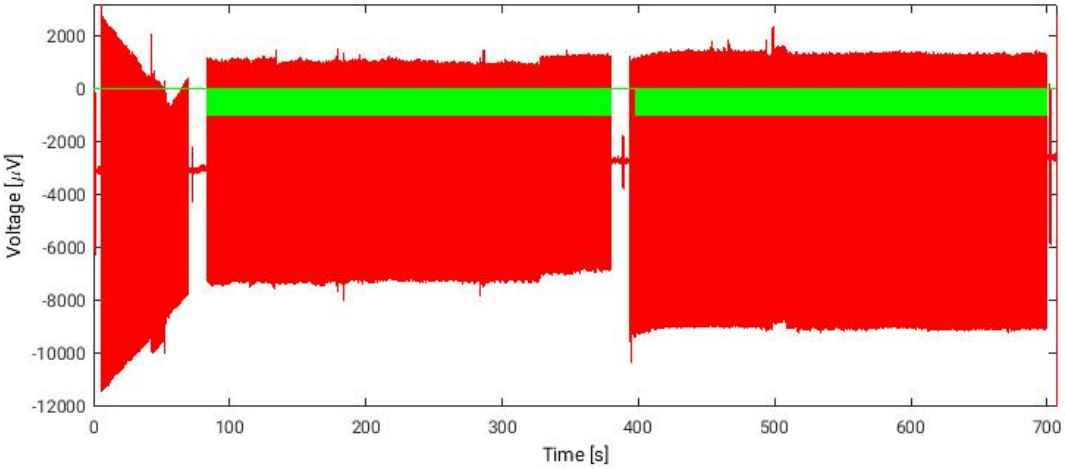

Figure 9: A typical collection of Electroencephalography (EEG) data during functional Magnetic Resonance Imaging (fMRI). Three imaging sequences were used here: a calibration procedure, a Magnetic Resonance Encephalography (MREG) sequence and a Multiband (MB) sequence. The green area shows time periods where trigger signals were collected from the scanner. The data is from an EEG-channel corresponding to F8 in the 10-20 system with reference to the common reference.

8 Results

In this chapter, statistical analyses are presented and results are illustrated in the same order as the data processing scheme outlined in Fig.8. The optimization steps taken to improve the algorithms are also described. The aim is to build a foundation for making conclusions on potential differences between the methods of artifact removal. All data processing is performed in MATLAB (The MathWorks, Inc.) and all algorithms outlined in the Methods chapter are implemented in the toolbox EEGLAB (Delorme and Makeig 2004).

The EEG-system used for data recording is a Sensor Net with 256 electrodes. When loading data into MATLAB there are 256 *channels*. Making comparisons between methods involving as many figures as there are channels would be more confusing than informative. Therefore, a subset of channels is selected for each hemisphere of the brain. The data from one of the two Mastoid channels, is then subtracted. When a channel is subtracted another channel it is called a *lead*.

Typically, when experts "sleep-score" EEG-data, i.e. characterize the stage of sleep a subject is in (see Section 6.1.4), three leads are looked upon: a frontal, central and an occipital lead. Examples are the channels from electrodes F3, C3 and O1 (see Fig.3) referenced to the Mastoid channel on the opposite hemisphere, namely M2. In this thesis, this scheme is repeated on both hemispheres. Tab.2 outlines the leads used for presenting results. It is the aim that using these leads throughout the thesis will make results easy to understand as well as representative for all channels. The reasons for choosing these 6 leads are that they collectively cover a large part of the scalp, and for sleep-scoring purposes these are often the leads of choice (Berry et al. 2012).

Frontal	Central	Occipital
F3-M2	C3-M2	O1-M2
F4-M1	C4-M1	O2-M1

Table 2: The Electroencephalography (EEG) leads used in this thesis. Uneven numbers are on the left side of the head, even numbers are on the right. Abbreviations are Frontal (F), Central (C), Occipital (O) and Mastoid (M).

8.1 Initial preprocessing

The first step of the data processing performed in this project is to cut out EEG-data recorded during an fMRI-sequence. Thus, the data shown in Fig.9 will be cut into two new data sets saved as individual files. There are 2 reasons for doing this:

- The morphology of the GA is dependent on the imaging sequence being used (see Fig.10). Since both methods for GA removal apply a moving average window, it would be a problem if the window used for removing artifacts recorded during one imaging sequence involved those of the other.
- The MRI-scanner does not send trigger signals when non-fMRI sequences such as calibration procedures are run (see Fig.9). Since both GA-removal methods (AAS and OBS) require a trigger signal, GA-removal in these time periods will not be possible.

As both AAS and OBS require a number of samples before the first and after the last artifact to be able to remove it, a full second (1000 samples) of the EEG and ECG data were kept both before the first and after the last trigger signal. The rest of the data processing is therefore done on 12 sets of EEG-data, where 7 were recorded during MREG and 5 during MB sequences. Whenever example data are illustrated in the remainder of the Results chapter, it is a data set with signals recorded during MREG imaging.

8.2 Gradient artifact removal

Choosing to remove GAs before correcting for BCG was natural due to the severity and exogenous nature of the GA compared to the BCG. Hence, GA removal is presented first. This is done by outlining how artifacts were removed, i.e. specifications of the algorithms, and then by comparing the two methods: AAS and OBS.

8.2.1 Algorithms and optimization

The two algorithms for GA removal are both implemented in the same function called *fmrib_fastr* by (Niazy et al. 2005). Since the difference between the two algorithms is whether or not PCA is used to estimate residuals after removing the moving average artifact, the choice to do PCA is simply omitted when using AAS.

In the algorithm, the combined EEG and ECG data are upsampled (interpolated) to a sampling frequency of 20kHz for better alignment of trigger signals to actual artifacts. For template construction, the data is bandpass-filtered with cut-off frequencies at 1Hz and 70Hz. A window length of 30 artifacts is used in the moving average estimation. For OBS,

the algorithm computes the number of principal components of the PCA on residuals to include in the template artifact for each channel.

In data, where GAs had been removed using AAS, sudden large amplitude spikes were observed in samples in the beginning and in the end of each data set. Further, for data where GAs and BCGs had both been removed using, sections of the resulting data showed "Not a Number" (NaN) values. It was found that removing the first and last two seconds of data after GA-correction as well as subtracting the mean of each channel solved these problems. To keep comparisons between the methods unbiased, removing the first and last part of the data, as well as demeaning, were done for data where GA correction had been done using OBS as well.

In Figs. 10-12, examples of 0.5 seconds of EEG-data from lead F3-M2 recorded during functional imaging are shown. The figures to the left show data recorded during an MREG sequence and to the right during an MB sequence. In Fig.11 the GAs have been removed using AAS and in Fig.12 the GAs have been removed using OBS.

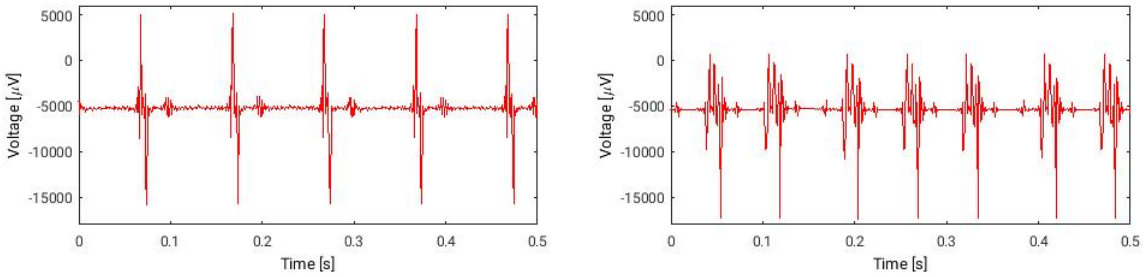

(a) **(b)**

Figure 10: Gradient artifacts (GA) in a 0.5 second period of Electroencephalography (EEG) data. (a): During Magnetic Resonance Encephalography (MREG) imaging. (b): During Multiband (MB) imaging. The lead shown is F3-M2.

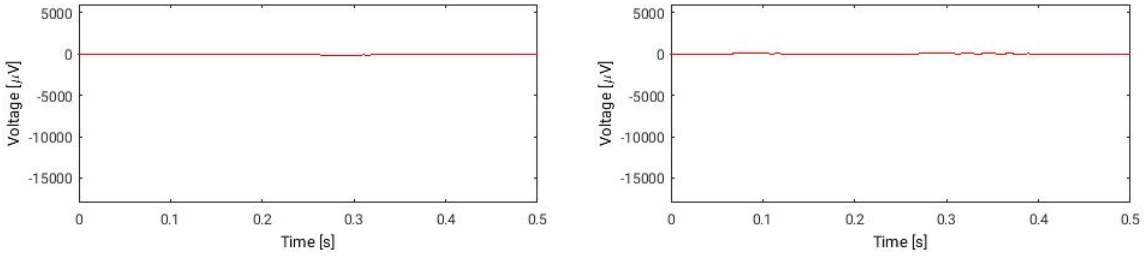

(a) **(b)**

Figure 11: GA-removal using AAS. 0.5 seconds of Electroencephalography (EEG) data after removing Gradient Artifacts (GA) using Average Artifact Subtraction (AAS). (a): During Magnetic Resonance Encephalography (MREG) imaging. (b): During Multiband (MB) imaging. The lead shown is F3-M2.

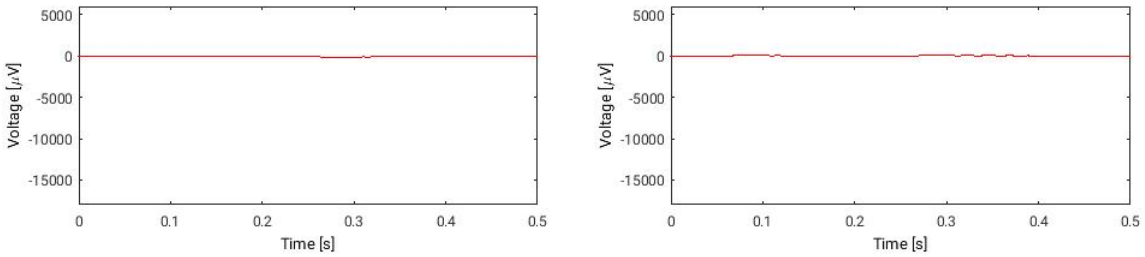

(a) **(b)**

Figure 12: GA-removal using OBS 0.5 seconds of Electroencephalography (EEG) data after removing Gradient Artifacts (GA) using Optimal Basis Sets (OBS). (a): During Magnetic Resonance Encephalography (MREG) imaging. (b): During Multiband (MB) imaging. The lead shown is F3-M2.

8.2.2 Comparison of gradient artifact removal methods

The first comparison is between one lead from data, where GAs have been corrected using AAS, and the same lead from data, where GAs have been corrected using OBS. The input to the two algorithms is the same data set. The Pearson correlation, which assumes that the data belongs to a Normal distribution, is computed for each lead listed in Tab.2. The argument for doing this comparison is that if the methods are different we should also see low correlations between the outputs of the two algorithms.

Scatter plots of all 12 data sets and 6 leads with the output from AAS on one axis and OBS on the other are seen in Figs.13-15. The linear fit on all curves is $y = 1.0 \cdot x + 0; r_{all} > 0.9999$. This means that the slope is unity and the intercept is zero.

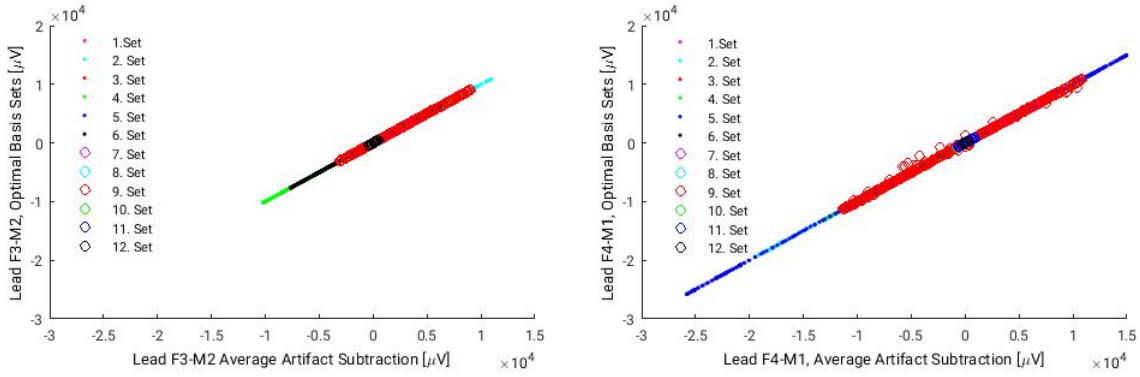

(a) **(b)**

Figure 13: Scatter plot of data from lead F3-M2 (a) and F4-M1 (b), where GA-correction has been carried out using Average Artifact Subtraction (AAS) and Optimal Basis Sets (OBS).

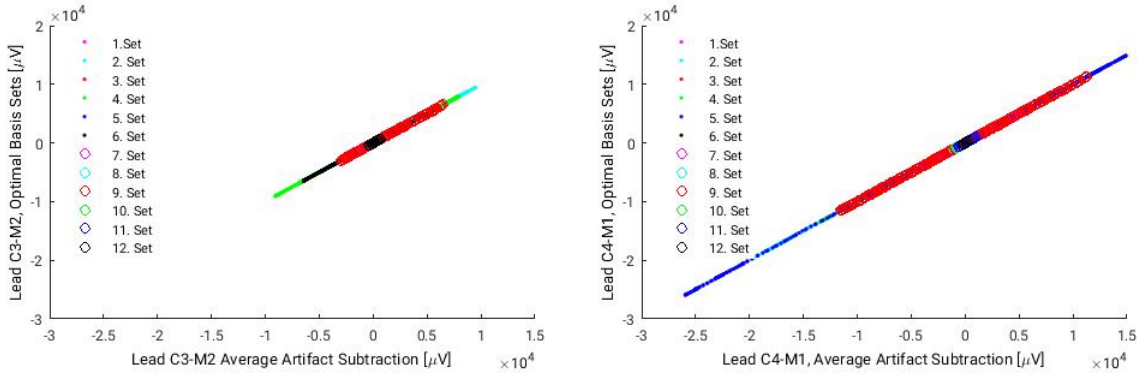

(a) **(b)**

Figure 14: Scatter plot of data from lead C3-M2 (a) and C4-M1 (b), where GA-correction has been carried out using Average Artifact Subtraction (AAS) and Optimal Basis Sets (OBS).

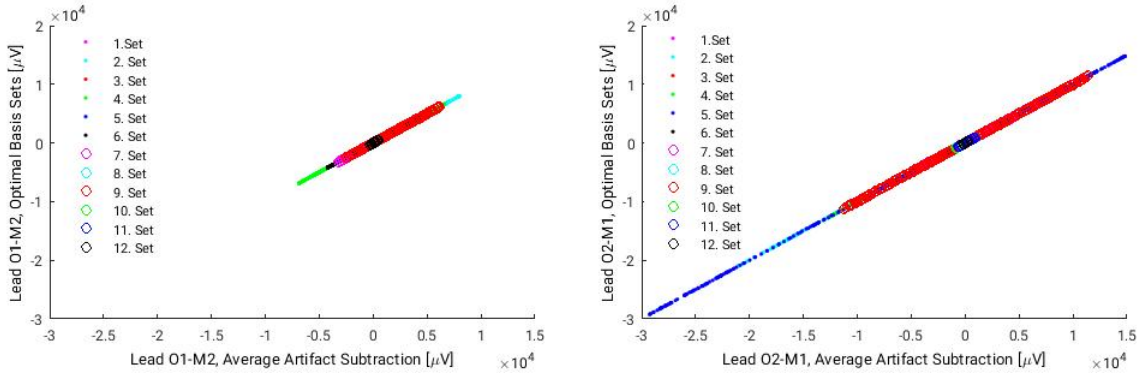

(a) **(b)**

Figure 15: Scatter plot of data from lead O1-M2 (a) and O2-M1 (b), where GA-correction has been carried out using Average Artifact Subtraction (AAS) and Optimal Basis Sets (OBS).

The mean and standard deviation of correlation coefficients are listed in Tab.3. From the table it is clear that data GA-corrected using AAS is correlated with the same data GA-corrected with OBS. However, the seemingly high correlation is bound to be affected by the underlying physiological signal, which is also exactly the same, since the input to the two algorithms is the same lead. Thus, conclusions drawn on these correlations alone would be inaccurate.

Therefore, other statistics will have to be used to strengthen any conclusions. An idea is to find the correlation between two different leads on data, where GAs have been corrected using AAS and compare it to the correlation between the same two leads on data, where GAs have been corrected using OBS. It is expected that the physiological electrical signals from the brain will be highly different in two leads that cover different areas of the brain. An example could be the comparison between lead C3-M2 and O2-M1 that cover different hemispheres and different lobes. If the correlation coefficient of the two leads in data with

AAS vs OBS	Mean	Standard deviation
F3-M2	0.99998	$9.8 \cdot 10^{-6}$
F4-M1	0.99999	$9.6 \cdot 10^{-6}$
C3-M2	0.99998	$9.9 \cdot 10^{-6}$
C4-M1	0.99997	$0.28 \cdot 10^{-6}$
O1-M2	0.99998	$9.9 \cdot 10^{-6}$
O2-M1	0.99999	$6.0 \cdot 10^{-6}$

Table 3: Mean and standard deviations for the 12 Pearson correlation coefficients (r) between 6 different leads for Average Artifact Subtraction (AAS) and the same 6 leads for Optimal Basis Sets (OBS). Note that the number of significant digits of the mean correlation does not follow scientific standards but were increased to show the magnitude of similarity between the two methods.

GA-correction using AAS is significantly different to that with GA-correction using OBS, then it may be an indicator that the two methods are different. With 6 leads there are a total of 15 combinations of leads, i.e. C3-M2 versus C4-M1, C3-M2 versus O2-M1 etc. As an example, two leads (C3-M2 and O2-M1) plotted against each other can be seen in Fig.16 for both methods of GA-correction. In both plots, slope and intercept of a linear regression model have been found as well as the Pearson correlation coefficient.

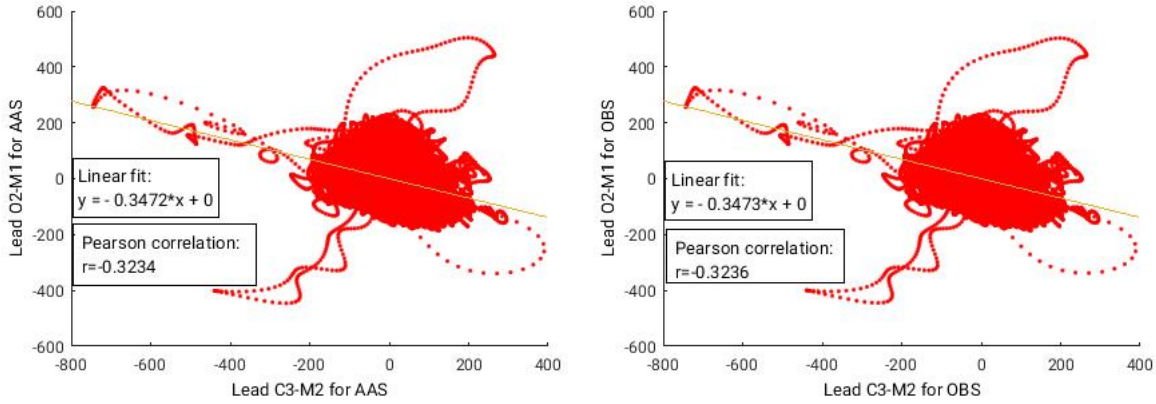

(a) **(b)**

Figure 16: Slope of linear fit and Pearson correlation coefficient between two different leads in Electroencephalography (EEG) data, where Gradient Artifacts (GA) have been corrected using (a): Average Artifact Subtraction (AAS), (b): Optimal Basis Sets (OBS). The number of significant digits deviates from what is used elsewhere in this thesis to show the size of difference between the two methods.

To quantify differences between correlation coefficients, Fisher's r-to-z transformation is used (Fisher 1915). This transformation calculates a z-score that can be applied to assess the significance of difference between two correlation coefficients that come from two different samples. The transformation is outlined in Eqs. 5-7.

$$z_1 = \frac{1}{2} \ln \frac{1 + r_1}{1 - r_1} \tag{5}$$

$$z_2 = \frac{1}{2} \ln \frac{1 + r_2}{1 - r_2} \tag{6}$$

$$z_{obs} = \frac{z_1 - z_2}{\sqrt{\frac{1}{N_1+3} + \frac{1}{N_2+3}}} \tag{7}$$

Here, r represents a correlation coefficient, z is the computed z-score and N is the number of samples in the data. The observed z-score computed in the last equation is compared with the critical value, which is 1.96 at a significance level of $\alpha = 0.05$. The p-value is computed by finding the probability of any z-score being higher than $|z_{obs}|$ in a normal distribution with mean $\mu = 0$ and standard deviation $\sigma = 1$, i.e. Eq.8.

$$p = 1 - 2 \cdot (|z| > z_{obs}) \tag{8}$$

The results of using Fisher's r-to-z transformation to compare the two GA-removal methods are collected in Tab.4. There is a p-value for every data set in every combination of leads. However, only the lowest among the 12 p-values in each combination of leads is shown.

Leads	F3-M2	F4-M1	C3-M2	C4-M1	O1-M2	O2-M1
F3-M2		0.46	0.096	0.44	0.66	0.43
F4-M1	0.46		0.43	0.36	0.42	0.15
C3-M2	0.096	0.43		0.50	0.52	0.31
C4-M1	0.44	0.36	0.50		0.45	0.60
O1-M2	0.66	0.42	0.52	0.45		0.74
O2-M1	0.43	0.15	0.31	0.60	0.74	

Table 4: The lowest p-values of Fisher's r-to-z transformation of correlation coefficients of combinations of the 6 leads. A significance level of $\alpha = 0.05$ is chosen.

A third method of comparison is to find the slope of the linear fit between the same same leads discussed above. The intercept should be zero, since the mean is subtracted after GA-correction using either of the two methods. An example of the slope of linear fit can also be seen in Fig.16. There are 12 slopes of linear fit for each combination of leads. The 12 slopes for GA-correction with AAS is subtracted the 12 slopes for GA-correction with OBS. The mean value and standard deviation of the differences in slopes is computed. For statistical comparison, a paired t-test assesses if two distributions are significantly different assuming normal distribution. Here, a distribution is the 12 slopes of linear fit between two leads in data, where GAs have been corrected using either AAS or OBS. An illustration of the lead with lowest p-value (C3-M2 vs C4-M1) can be seen in Fig.17.

Lead 1	Lead 2	$\mu_{a1} - \mu_{a2}$ $(\cdot 10^{-3})$	σ $(\cdot 10^{-3})$	p-value
F3-M2	F4-M1	-0.36	1.5	0.42
F3-M2	C3-M2	0.11	0.24	0.14
F3-M2	C4-M1	0.047	0.77	0.84
F3-M2	O1-M2	0.13	0.18	0.027*
F3-M2	O2-M2	-0.11	1.0	0.72
F4-M1	C3-M2	0.25	0.30	0.016*
F4-M1	C4-M1	-0.26	0.82	0.30
F4-M1	O1-M2	0.23	0.31	0.023*
F4-M1	O2-M2	-0.23	0.70	0.28
C3-M2	C4-M1	0.22	0.24	0.0084*
C3-M2	O1-M2	0.20	0.24	0.015*
C3-M2	O2-M2	-0.027	0.16	0.57
C4-M1	O1-M2	0.073	0.37	0.51
C4-M1	O2-M2	0.38	0.48	0.019*
O1-M2	O2-M2	0.17	0.92	0.54

Table 5: Slopes of linear fit between two leads. The mean difference between slopes between Gradient Artifact (GA) correction with Average Artifact Subtraction (AAS) and Optimal Basis Sets (OBS) as well as the standard deviation and p-value are shown. An asterisk (*) denotes a significant difference.

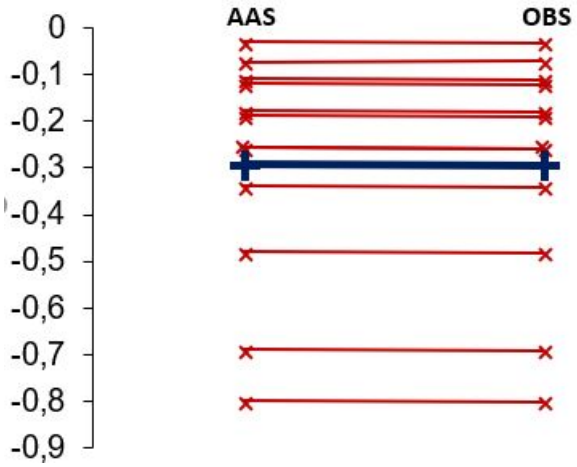

Figure 17: Slopes in the lead C3-M2 versus C4-M1 after Gradient Artifact (GA) removal with Average Artifact Subtraction (AAS) and Optimal Basis Sets (OBS). The blue line is the mean value of slopes of AAS and OBS, respectively.

8.3 QRS-detection

The QRS-detection algorithm developed by (Christov 2004) and expanded by (Niazy et al. 2005) is implemented in EEGLAB as a function with the name *fmrib_qrsdetect*. As mentioned in the Methods chapter, the algorithm uses the kTEO to separate R-peaks from the rest of

the ECG signal. The value of k is computed according to Eq.3. Unfortunately, a fault in the algorithm caused it to detect twice the amount of peaks that were visible in the ECG signal. This was seen in several data sets and had the effect of inaccurate subsequent BCG-removal using either of the three BCG-removal methods. To solve this problem, two things had to be changed:

1. The ECG-signal was high-pass filtered "manually" with an ideal filter. That is, the signal was transformed to the Fourier domain (or, frequency domain) and frequencies below $0.5Hz$ were set to zero. Doing manual filtering is only possible in offline signal processing and a consequence of doing this is lack of knowledge on the phase characteristics of the ideal filter.

2. It was discovered that the value k in the kTEO had a possibility to be zero in the *fmrib_qrsdetect* algorithm. If this happens, Eq.2 reduces to the following:

$$\mathbf{X}[n] = \mathbf{E}^2[n] - \mathbf{E}[n-0]\mathbf{E}[n+0] = \mathbf{E}^2[n] - \mathbf{E}^2[n] = 0$$

   The algorithm is therefore modified with an if-else statement setting $k = 1$ if it had computed k to be zero. $k = 1$ was chosen arbitrarily.

The modifications solved the double-detection problem. After this, the main flaws of the QRS-detection algorithm were at time points of head movement and in the beginning and end of each data set. Here, a couple of R-peaks were not detected. Out of approximately 300 heartbeats per ≈ 5 minute data set (with 60 beats per minute) a maximum of 5 mistakes were observed across all 12 data sets. A mistake is here defined as either a missing peak or wrongly detected peak.

An example of 15 seconds of GA-free ECG data with detected R-peaks can be seen in Fig.18.

8.4 Ballistocardiogram removal

Due to the less exogenous nature of the BCG than the GA, using a moving average template approach may prove to be less feasible. ICA on the other hand does assume temporal relation between adjacent artifacts. An important thing to remember is that AAS and OBS remove artifacts *per channel* whereas ICA computes independent components that are present in all channels, albeit to different extents.

8.4.1 Average Artifact Subtraction and Optimal Basis Sets

Removal of BCG using AAS and OBS is done using the algorithm called *fmrib_pas* (Niazy et al. 2005), which has two options: 'mean' for a moving average procedure alone, and 'OBS' for a combination of a moving average approach and PCA. For BCG-correction using OBS, contrary to GA-correction, the option for automatically chosen amount of principal components is not available. 4 principal components were chosen for all channels as this was recommended by the author of the original article. The algorithm takes GA-free data and a vector of ones at time points of detected R-peaks and zeros otherwise as inputs.

8.4.2 Independent Component Analysis

The ICA-algorithm, called *runica*, was implemented in EEGLAB by (Delorme and Makeig 2004). This algorithm takes all 256 EEG-channels (not ECG) as input. The outputs are matrices from which independent components of same length as the input channels can be computed. An example showing 15 seconds of the first 10 independent components after running ICA on the example-EEG data (during an MREG sequence) can be seen in Fig.18. A black line is placed at the first detected R-peak of the ECG-signal of the same data set. Notice the small delay from R-peak to maxima in the independent components with BCG-contribution, e.g. components 2 and 5. After running the algorithm, one has to scroll through all 256 components to identify components with possible contribution from BCG. This can be a time consuming process, and since the algorithm takes time to run (several hours), all in all it would be better if it could be done automatically or at least semi-automatically.

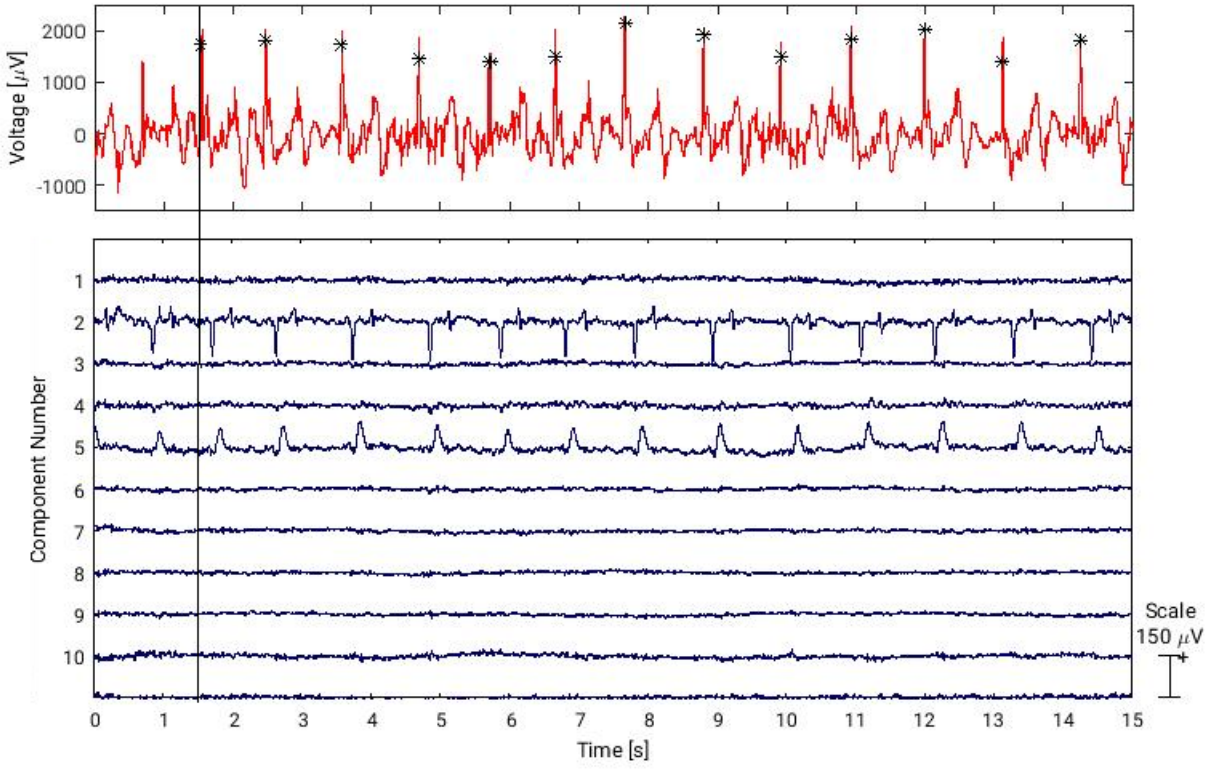

Figure 18: 10 out of 256 independent components after running Independent Component Analysis (ICA) on Electroencephalography (EEG) data recorded during an Magnetic Resonance Encephalography (MREG) sequence. The Electrocardiogram (ECG) signal free from Gradient Artifacts (GAs) from the same data set and same time period is seen on the top. Black stars indicate a detected R-peak. The black line indicates the first detected R-peak.

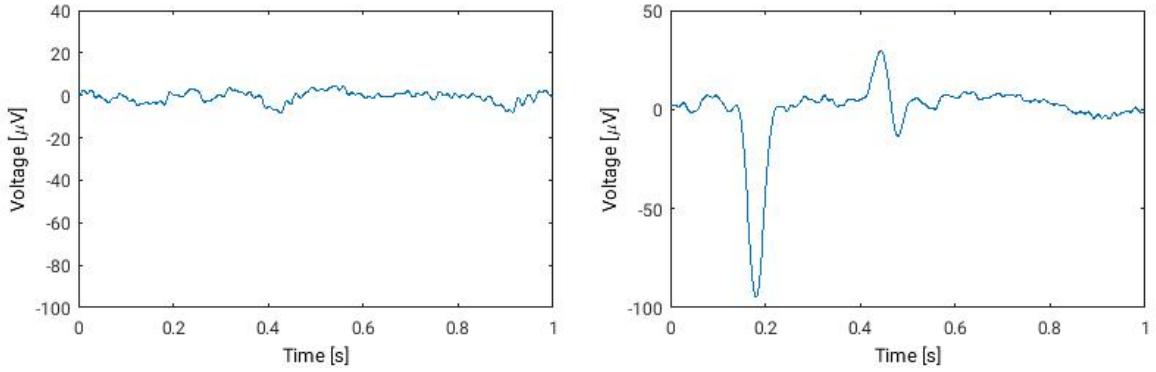

(a) **(b)**

Figure 19: Independent Component 1 (a) and 2 (b) from the same data divided into equal sized segments starting at time points of detected R-peaks. The average across all segments is shown. Note there are as many segments as detected QRS-complexes.

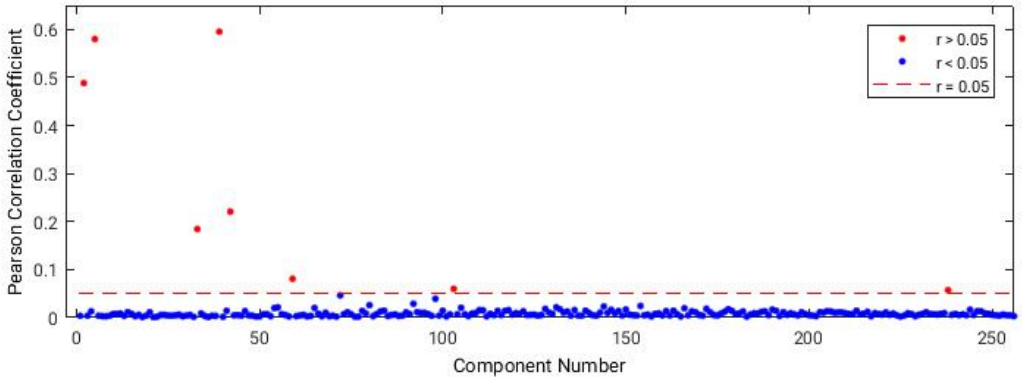

Figure 20: Pearson correlation coefficients between independent components and their respective repeated averaged artifact segments. Red markers for components with correlation coefficients above threshold of $r = 0.05$, blue for below threshold.

The proposed extension to ICA is made to run automatically. It is made as a MATLAB-script that takes the same vector of zeros and ones of detected QRS-complexes as *fmrib_pas* as input together with the independent components computed in the previous step. The procedure of the algorithm is outlined in Section 6.3.5. The averaged heartbeat segments for the first two components are shown in Fig.19. These averaged segments are computed for all components and are repeated to have the same length as the corresponding component. The Pearson correlations are then computed. An example of the Pearson correlation coefficient between each component and its repeated averaged heartbeat segment is shown in Fig.20.

An example of the topography of component 2 in Fig.18, i.e. the component with average heartbeat segment in Fig.19b, is shown in Fig.21.

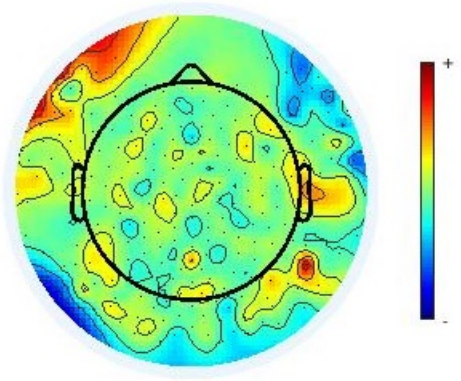

Figure 21: The topography of independent component number two of an Independent Component Analysis (ICA) on an Electroencephalography (EEG) data set recorded during Magnetic Resonance Encephalography (MREG) imaging.

An example showing the first 15 seconds of lead F3-M2 of a data set recorded during MREG imaging (same as all example figures in this chapter) is shown in Fig.22. The top subfigure shows EEG-data after GA-correction but before BCG-correction. The second subfigure shows the data after BCG-correction with AAS, the third after BCG correction using OBS and the fourth after BCG-correction with ICA. In the latter case, independent components having a correlation coefficient with their repeated average artifact segment above the threshold of $r = 0.5$, i.e. the red dots in Fig.20 have been removed. All data in Fig.22 have been filtered with a Chebyshev filter with cut-off frequencies at $0.5Hz$ and $40Hz$

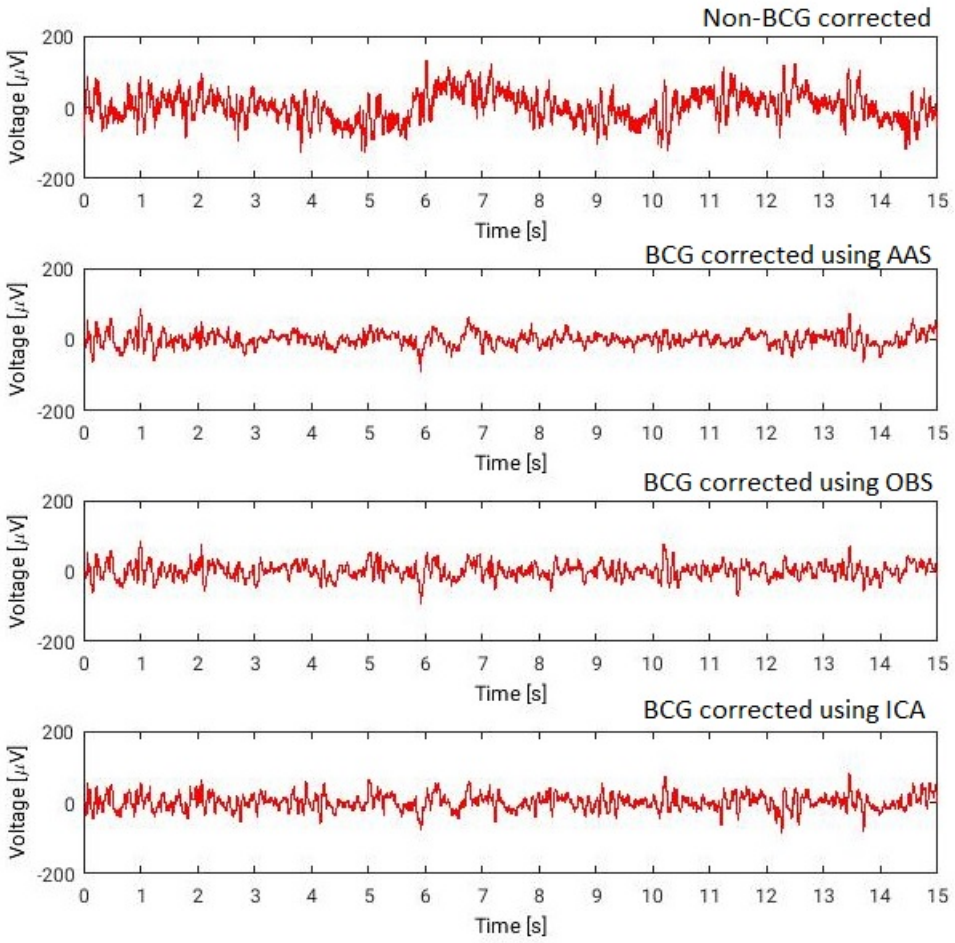

Figure 22: 15 seconds of Electroencephalography (EEG) data from lead F3-M2. Top: Before correction for Ballistocardiogram (BCG). Second: After BCG-correction using Average Artifact Subtraction (AAS). Third: After BCG-correction using Optimal Basis Sets (OBS). Bottom: After BCG-correction using Independent Component Analysis (ICA). All data in this figure have been filtered using a Chebyshev bandpass filter with cut-off frequencies at $0.5Hz$ and $40Hz$.

8.4.3 Comparison of Ballistocardiogram removal methods

The same three statistical analyses used for comparing GA-removal methods will be used to compare BCG correction methods. The difference is that there are now three comparisons - AAS versus OBS, AAS versus ICA and OBS versus ICA. This calls for three times the amount of illustrations, hence, some graphs and tables will be collected in the Appendix.

The first analysis is between a lead in data BCG-corrected using one method and the same lead in the same data BCG-corrected using another method. The Pearson correlation coefficient between the two methods is computed for all data sets and all leads. The mean and standard deviations for each lead across the 12 data sets are shown in Tab.6 for AAS vs OBS, Tab.7 for AAS vs ICA and Tab.8 for OBS vs ICA. Scatter plots of all 12 data sets and 6 leads are shown in the Appendix: Fig.24 for AAS vs OBS, Fig.25 for AAS vs ICA and

Fig.26 for OBS vs ICA. However, an example of the scatter plot for lead C4-M1 for all three comparisons can be seen in Fig.23.

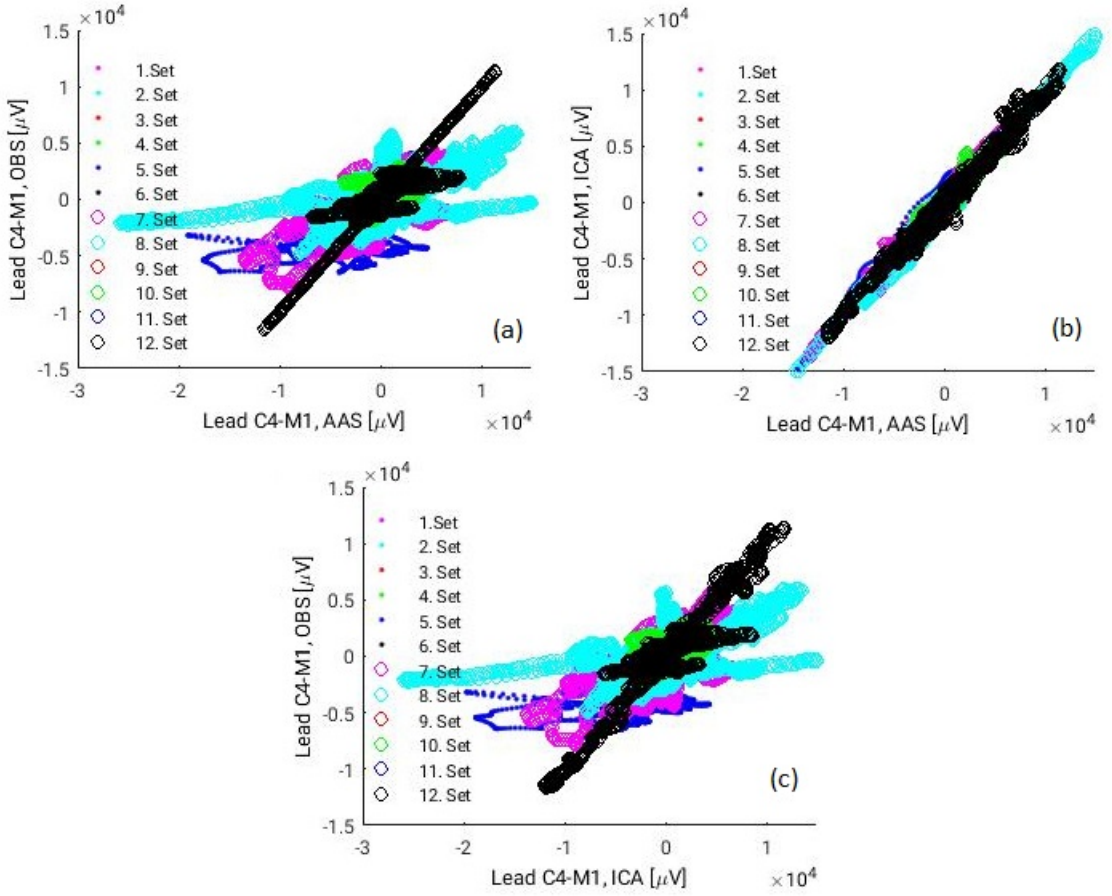

Figure 23: Scatter plot of lead C4-M1 for all three comparisons. (a) Average Artifact Subtraction (AAS) versus Optimal Basis Sets (OBS). (b): AAS versus Independent Component Analysis (ICA). (c): ICA versus OBS.

AAS vs OBS	Mean	Standard deviation
F3-M2	0.80	0.11
F4-M1	0.78	0.13
C3-M2	0.77	0.12
C4-M1	0.79	0.13
O1-M2	0.77	0.091
O2-M1	0.79	0.14

Table 6: Mean and standard deviations for the 12 Pearson correlation coefficients (r) between 6 different leads for Ballistocardiogram (BCG) correction using Average Artifact Subtraction (AAS) and the same 6 leads using Optimal Basis Sets (OBS).

AAS vs ICA	Mean	Standard deviation
F3-M2	0.91	0.058
F4-M1	0.91	0.069
C3-M2	0.90	0.073
C4-M1	0.93	0.036
O1-M2	0.89	0.076
O2-M1	0.91	0.066

Table 7: Mean and standard deviations for the 12 Pearson correlation coefficients (r) between 6 different leads for Ballistocardiogram (BCG) correction using Average Artifact Subtraction (AAS) and the same 6 leads using Independent Component Analysis (ICA).

OBS vs ICA	Mean	Standard deviation
F3-M2	0.75	0.093
F4-M1	0.74	0.11
C3-M2	0.71	0.093
C4-M1	0.76	0.11
O1-M2	0.72	0.069
O2-M1	0.75	0.12

Table 8: Mean and standard deviations for the 12 Pearson correlation coefficients (r) between 6 different leads for Ballistocardiogram (BCG) correction using Optimal Basis Sets (OBS) and the same 6 leads using Independent Component Analysis (ICA).

In the second analysis, the correlation coefficient is computed between one lead on data, where BCG-correction has been carried out using AAS, and a second lead on the same data. As mentioned, there are 15 combinations of leads per data set and a correlation coefficient is computed for each combination of leads and each data set. Fisher's r-to-z transformation is then calculated and each z-score is compared with the corresponding z-score in the same lead, same original data, but another BCG-removal method, and a p-value is computed. In Tab.9 the amount of p-values showing a significant difference ($p < 0.05$) per combination of leads and methods is collected.

Lead 1	Lead 2	AAS vs OBS	AAS vs ICA	OBS vs ICA
F3-M2	F4-M1	all	10 of 12	all
F3-M2	C3-M2	all	all	all
F3-M2	C4-M1	11 of 12	11 of 12	all
F3-M2	O1-M2	all	9 of 12	all
F3-M2	O2-M2	10 of 12	10 of 12	all
F4-M1	C3-M2	all	all	all
F4-M1	C4-M1	all	7 of 12	all
F4-M1	O1-M2	all	all	11 of 12
F4-M1	O2-M2	10 of 12	all	all
C3-M2	C4-M1	all	all	all
C3-M2	O1-M2	all	11 of 12	all
C3-M2	O2-M2	all	9 of 12	all
C4-M1	O1-M2	all	11 of 12	all
C4-M1	O2-M2	all	10 of 12	all
O1-M2	O2-M2	all	11 of 12	all

Table 9: The amount of p-values of Fisher's r-to-z transformation that are below the significant value of $\alpha = 0.05$. Every row is a new combination of leads. In every combination of leads and combination of methods there are correlations for 12 data sets that are compared using Fisher's r-to-z transformation.

Lastly, the third analysis is between slopes of linear fit of the same leads as discussed above. A linear regression is carried out on all combinations of leads for each method. The mean difference between the slopes of two methods, as well as the standard deviation of the difference and p-value of a paired t-test is computed. Tab.10 shows results for comparison between BCG correction using AAS and OBS, Tab.11 for AAS and ICA and Tab.12 for OBS and ICA, all in the Appendix.

9 Discussion

Conducting studies using simultaneous EEG and fMRI is a prime opportunity for researchers to combine strengths of two modalities. EEG offers real-time observation of electrical activity in the cortex of the brain with high temporal resolution. For sleep observation purposes, guidelines exist for decoding EEG-signals, and the modality is therefore often the method of choice. However, EEG cannot reveal underlying physiological processes that initiate, or are initiated by, sleep. Functional imaging such as fMRI offers researchers a tool to "look inside the brain" and see levels of metabolic activation in subjects with relatively high spatial resolution.

The larger project that will investigate a vascular network enhanced during sleep (the GS) that this thesis is part of, conducts its data recording using simultaneous EEG-fMRI. Test subjects are scanned three days while wearing an EEG electrode net with 256 electrodes. Two of these days the subjects are sleep deprived, and the hope is that they will fall asleep inside the scanner, despite the noisy environment of the MRI-scanner and discomfort of lying with the head on top of EEG-electrodes. Two different fMRI-sequences are run interchangeably over a 30-minute period in order to image the brain as the subject falls asleep. The EEG-signals from the studies will be examined to locate changes, e.g. sleep characteristics as outlined in Sec.6.1.4, and the fMRI-images will subsequently be investigated to observe physiological changes in the transition to sleep. Thus, the combination of EEG and fMRI is ideally suited for this project. The major drawback of combining the two modalities is the presence of artifacts in the EEG-signal. Of several different artifacts the GA and BCG are the most prominent ones.

9.1 Gradient artifacts

The GA occurs whenever switching of magnetic gradients of the MRI-scanner happens, i.e. when an image is taken. This results in steeply rising transients and high-voltage peaks of magnitude more than 100 times what is normally seen in EEG-signals. At first glance, this artifact completely disrupts the signal (see Fig.9). However, the GA is caused by the physical properties of the MRI-scanner and shows very little variation between adjacent artifacts. The only major variations in the GA are head movements, either slow involuntary movement resulting from the subject getting to rest inside the scanner, or fast voluntary movement. The latter can, to some extent, be prevented by making sure the subject is as comfortable as possible in the MRI-scanner. However, the morphology of the GA does change from channel to channel.

In this thesis two methods are tested for GA-removal: AAS (Allen, Josephs, and Turner 2000) and OBS (Niazy et al. 2005). These are the two methods most used in the literature. They both rely on the same principle in that a template artifact is constructed using a moving average of the (in this thesis) 30 nearest neighboring artifacts. The starting point of single artifacts are determined by a trigger signal sent from the MRI-scanner. Template construction is done separately for all channels, and the use of a moving average procedure guards against the slow involuntary movements that may change the morphology of the GA. OBS is an expanded version of AAS that combines the moving average with a PCA on the signal after subtraction of the template artifact. The aim of adding PCA to the estimation of artifacts is to lessen residual artifacts.

In the Methods chapter, a possibility to only include artifacts in the template if they are well correlated with the rest in the moving average window was discussed. Due to time limitations, this was not included. If implemented, this addition to the algorithm could lessen residual artifacts after template subtraction.

In Fig.10, GAs during half a second of imaging with MREG and MB scanning can be seen. In Figs.11 and 12 the artifacts have been removed using AAS and OBS. The scaling on the axes were kept constant throughout the plots to illustrate the magnitude of the signal after GA-correction compared to before. Figs.11 and 12 reveal no visible differences between the two artifact removal methods.

9.2 Ballistocardiographic artifacts

In contrast to the GA, the BCG is of less exogenous character. While caused by the strong static magnetic field of the MRI-scanner, its morphology and periodicity depends on the heart. The morphology is changed by several things, such as the stroke volume of the heart or the resistance of vessels carrying blood to the scalp causing the skin to vibrate and electrodes to move. The periodicity is dependent on the heart rate and events such as a skipped heart beat do occur. Head movements affect the BCG in the same way as they affect the GA.

Three methods are tested for BCG-correction: AAS (Allen, Josephs, and Turner 2000), OBS (Niazy et al. 2005) and ICA (Makeig et al. 1996). The two first methods work the same way for BCG-removal as they do for GA-removal, with the exception that automatically chosen number of principal components for estimation of residual artifact after removing the moving average template is not available in the algorithm for BCG-removal using OBS. Further, the detected R-peaks from the QRS-detection algorithm are all moved 210ms ahead in time to account for the delay from heartbeat to fluctuations in the EEG-signal.

ICA is fundamentally different from AAS and OBS. Primarily, the algorithm was not developed for artifact removal purposes only, but for blind source separation of independent activities of the brain, i.e. physiological phenomena. Secondly, it produces independent components that are present, to different extents, in all channels and thus does not operate channel-wise. Under the assumption of equal delay from heart beat to BCG in all channels, as well as equal morphology of the artifact, ICA would ideally produce a single independent component with BCG-contribution that is present in all channels. However, these assumptions do not necessarily hold true and instead, several independent components (between 4-18 per data set) showed visually identifiable contribution from BCG. An example of the first 10 of 256 independent components from the example data set is visualized in Fig.18. The corresponding ECG-signal with detected R-peaks marked is shown in the same figure to illustrate the delay between R-peak and maxima in the independent components.

The high variability in the number of independent components with BCG-contributions may pose a problem regarding the similarity of the algorithm between data sets. If ICA were to be the method of choice for BCG-correction, a certainty in the similarity in the amount of removed artifact should be expected. Whether or not this is the case is a subject for further analysis. Both regarding inter-data set and inter-subject comparison.

An example of the topography of an independent component with BCG-contribution is shown in Fig.21. The topography of a component shows where on the scalp it is located, and it can have both positive and negative polarity. Ideally, this figure would have shown the average topography of all components above threshold in Fig.20. An average topography

could be a supplement to the analysis of ICA mentioned above. If the average topography is different between data sets or between subjects, then it would be an indicator of unwanted high variability between outputs of ICA.

Instead of manually scrolling through all independent components computed by the algorithm, an extension is proposed that automatically decides which components have contributions from heart beat. The algorithm segments each component into N equal sized vectors of length equal to the amount of samples in an average heartbeat. That is, the QRS-detection algorithm produces a vector of N ones at time points of detected R-peaks and zeros otherwise. The average number of samples between each detected R-peak is computed, in most cases approximately 1000 samples corresponding to one second. The N potential heart beat segments are then averaged. Examples are shown in Fig.19. Finally, these averaged heart beat segments are repeated at time points of detected R-peaks to have the same length as the independent component, and the Pearson correlation between the repeated averaged heart beat segment and the corresponding independent component is computed. Components having a correlation coefficient above $r = 0.05$ are selected and removed from the EEG data. An example is illustrated in Fig.20.

Using this extension to ICA has two advantages compared to not using it. First, one does not have to spend time scrolling through all components to identify those with contribution from BCG. Secondly, this method lessens differences between the performance of ICA between data sets, in that a constant measure is used to identify components with contribution from BCG. For some components it can be difficult to spot if there are heart beat contribution. If one had to manually select components to remove, there would inarguably be differences in how visible the contribution should be between data sets. The disadvantage of using the method is deciding correct threshold. Originally, it was desired to do statistical comparisons between potential thresholds, but shortage of time made it necessary to select a single threshold. The threshold coefficient was chosen using a trial-and-error approach, i.e. setting a threshold and evaluating if the independent components with correlation coefficient above the threshold corresponded to the ones that would have been manually selected. The threshold coefficient $r = 0.05$ was believed to be the best compromise.

An example of a data set, where GAs have been removed using AAS, and where BCG-correction has been carried out using either AAS, OBS or the extended ICA is shown in Fig.22. Here all data have been bandpass filtered using a Chebyshev filter for visualization purposes. This filtering attenuates low frequencies, e.g. the respiratory cycle, and smoothes the signal by attenuating high frequencies. The ECG-data corresponding to the same time period is seen in Fig.18, and it reveals that the first R-peak was not detected. Thus, neither AAS nor OBS were able to remove the first ballistocardiographic artifact. It is difficult to spot if the three methods are different. Thus, statistical comparisons are necessary.

9.3 Comparison of methods

Figuring out which method removes artifact better than the other is difficult, since we do not have a ground truth signal. That is, we have no way of knowing what a signal corrupted with artifacts would look like if it was free from artifacts and only contained physiological information (and noise). Therefore, choosing how to compare artifact removal methods has been a main topic of discussion throughout the project period. Due to time limitations, it was settled to determine whether or not the methods are significantly different by doing

statistical comparisons between the methods.

- As explained in the Results chapter, the first comparison is between two artifact removal methods using the same lead and the same original data. The Pearson correlation coefficient is computed between the two methods for all leads listed in Tab.2 and for all 12 data sets. This is the most simple comparison study, but it is imperfect since potential similarities are bound to be affected by the underlying physiological electrical signals, which theoretically should be exactly the same. Hence, other analyses have to be made to keep comparisons unbiased.

- The second comparison is to compute the Pearson correlation coefficient between two leads on a data set, where the artifacts have been removed using one method. The same is done for the same two leads and the same original data set, but after another artifact removal method has been used. The two computed correlation coefficients are then compared using Fisher's r-to-z transformation, and a p-value is found. There are p-values for all 15 combinations of leads and all 12 data sets. If two correlation coefficients are found to be significantly different, then it may be an indicator that the two methods are different.

- The third comparison is between slopes of the linear regression between two leads that come from the same data set and where artifacts have been removed using the same method. A linear regression is also found between the same two leads that come from the same original data set, but where the artifacts have been removed using a different method. There are 12 slopes of linear regression per combination of leads and per artifact removal method. The 12 slopes in each combination of leads for one method is subtracted those of the other, and the mean and standard deviation is found. This comparison resembles the one above, but differs in that a paired t-test is used to find a p-value, the interpretation of which determines if the methods are significantly different. Only one p-value is computed per combination of leads.

The second and third comparison are illustrated in Fig.16. Using these three comparisons, it is the aim to determine if artifact removal methods are different from each other. Thus, this thesis will *not* make any conclusion on which method is the *best*.

9.3.1 Comparison of gradient artifact removal methods

Figs. 13 to 15 show the first comparison, where the same lead after GA-correction using the two methods are plotted against each other. Only Fig.13b shows data points that lie outside the otherwise straight line. The linear regression on all these plots was found to have unity slope and zero intercept. This indicates that the two methods are very similar. Tab.3 shows the Pearson correlation coefficients for the first comparison. An extra amount of significant digits had to be included to show the magnitude of similarity between AAS and OBS for GA removal. The high correlation coefficients as well as very low standard deviations indicate high similarity between the two methods.

Results from the second comparison are collected in Tab.4 that only shows the *lowest* p-value among 12 data sets. Thus, no significant differences were found between correlation coefficients from either of the two methods.

Results from the third comparison between slopes of linear regression are collected in Tab.5. We see that the mean differences between slopes are quite small for all combinations of leads. However, the standard deviations are also quite small. For this reason, the paired t-test proved significant difference between slopes for 6 out of 15 combinations of leads. An example of the lead with the lowest p-value is shown in Fig.17. This figure, showing the lead where the two methods proved to be the least similar, illustrates the difference between slopes of the two methods. When taken under closer consideration, it was seen that, although very small, all the differences were positive. This, and the very low standard deviation of differences made the paired t-test compute a significantly low p-value. It is therefore decided that the low p-values of Tab.5 do not mean that the methods are different.

9.3.2 Comparison of ballistocardiogram removal methods

The same three comparisons are made for the BCG removal methods. However, since there are three methods, each one will be compared with both of the other methods. That is, the following combinations are made: AAS versus OBS, AAS versus ICA and OBS versus ICA.

Figs. 24 to 26 in the Appendix show the first comparison, where two methods are plotted against each other. Fig.23 shows an example of one lead in all three combinations of methods. In Fig.24 and 26 we see collections of data points that are not nearly as well placed on a straight line as was the case for GA-correction. However, in Fig.25, i.e. AAS versus ICA, the two methods resemble each other more. This could either mean that AAS and ICA remove BCGs in a similar way or that they both remove artifacts poorly and only data after BCG-correction using OBS showed a substantial change compared to before BCG-correction. The correlation coefficients in Tabs. 6 to 8 tell the same story. Mean correlation coefficients in comparisons where OBS is one of two methods are lower than for AAS versus ICA. Likewise, standard deviations are generally higher.

In comparison two, where combinations of leads are examined and correlation coefficients computed, the results are collected in Tab.9. As there are 12 p-values for every combination of methods and combination of leads, it is chosen to only show the amount of p-values that show significant differences. Only 6 out 360 p-values that includes BCG removal using OBS did not show significant difference. In the comparison between AAS and ICA, it can be seen that most of the p-values show significant difference, but not as many as in comparisons with OBS.

Results from comparison three that includes slopes of linear regression are collected in Tabs. 10 to 12. Here only 2 out of 45 p-values were less than the significant value of $\alpha = 0.05$. Compared to GA-correction, it is curious that there are next to no significant differences between BCG-removal methods. However, as was the case for the GA-removal comparison, standard deviations play a role when it comes to computing t-tests. in this case, all standard deviations are fairly high compared to the mean of the difference in slopes.

9.4 QRS-detection

Originally, it was not the intention for this thesis to discuss detection of QRS-complexes and the corresponding R-peaks of ECG signals. The algorithm chosen for this problem was recommended by (Niazy et al. 2005). However, successful detection of R-peaks is a prerequisite for correct BCG-removal using AAS, OBS or the proposed extended version of

ICA. For some data sets, the QRS-detection algorithm detected twice the number of peaks. After high-pass filtering the ECG signal as well as implementing some lines of code in the algorithm, the problem was solved.

9.5 Conclusion

It was the aim of this bachelor thesis to compare methods for removal of the two most prominent EEG-artifacts in simultaneous EEG-fMRI studies: The GA and the BCG.

Two methods were compared for the removal of GAs: AAS (Allen, Josephs, and Turner 2000) and OBS (Niazy et al. 2005). The resulting data from GA-correction using the two methods are highly correlated, and using Fisher's r-to-z transformation revealed no significant differences. Slopes of linear fit revealed some significant differences, but these were mediated by very low standard deviations in the differences of slopes between the two methods. It is concluded that the two methods *are not* significantly different.

Three methods were compared for BCG-correction: AAS (Allen, Josephs, and Turner 2000), OBS (Niazy et al. 2005) and ICA (Makeig et al. 1996). The three methods were not as highly correlated, and Fisher's r-to-z transformation revealed significant differences in nearly all analyses of correlations. Analysis of differences in slopes of linear regression showed very few significant values, but these were mediated by fairly high standard deviations compared to the GA comparison. AAS and ICA were more alike than OBS was with either AAS or ICA, both in terms of correlations and slopes. Whether this means that AAS and ICA remove BCGs successfully or poorly in similar ways is a subject for further studies. It is concluded that the three methods are all significantly different from each other.

9.6 Future Perspectives

Time is often a major limitation in projects that have deadlines. Many analyses could have been made in order to optimize the artifact removal algorithms. To name a few:

- Different QRS-detection algorithms could be applied and their success rates analyzed to enhance conditions for BCG removal.
- OBS for BCG-correction could be including different amounts of principal components in the template artifact.
- In the proposed extension to ICA a correlation threshold of $r = 0.05$ was chosen using a trial-and-error approach. Further analyses could determine whether this is the best threshold.

Furthermore, this thesis was only able to determine if methods for artifact removal are different. To determine which is the better method, the fact that the data were recorded for a sleep study makes comparison using sleep scoring on EEG a possibility. This could include spectral analysis of EEG channels or expert opinions.

Further analysis on whether ICA is a stable method of artifact removal is needed. The topography of independent components with BCG-contribution can be used for comparison between data sets and between subjects.

Finally, there have been proposed other methods of artifact removal in the literature, such as Harmonic Regression (Krishnaswamy et al. 2016). A more comprehensive analysis of artifact removal methods could include these methods.

References

[1] Philip J. Allen, Oliver Josephs, and Robert Turner. "A method for removing imaging artifact from continuous EEG recorded during functional MRI". In: *NeuroImage* (2000). ISSN: 10538119. DOI: 10.1006/nimg.2000.0599.

[2] MF Bear, BW Connors, and MA Paradiso. *Neuroscience*. 2007. ISBN: 9780878937431. DOI: 978-0878937257.

[3] A J Bell and T J Sejnowski. "An information-maximization approach to blind separation and blind deconvolution". In: *Neural computation* (1995). ISSN: 0899-7667. DOI: 10.1162/neco.1995.7.6.1129.

[4] Richard B. Berry et al. "Rules for scoring respiratory events in sleep: Update of the 2007 AASM manual for the scoring of sleep and associated events". In: *Journal of Clinical Sleep Medicine* (2012). ISSN: 15509389. DOI: 10.5664/jcsm.2172.

[5] I.I. Christov. "Real time electrocardiogram QRS detection using combined adaptive threshold". In: *BioMedical Engineering Online* (2004). ISSN: 1475925X. DOI: 10.1186/1475-925X-3-28.

[6] Arnaud Delorme and Scott Makeig. "EEGLAB: An open source toolbox for analysis of single-trial EEG dynamics including independent component analysis". In: *Journal of Neuroscience Methods* (2004). ISSN: 01650270. DOI: 10.1016/j.jneumeth.2003.10.009.

[7] Tom Eichele et al. "Removal of MRI Artifacts from EEG Recordings". In: *Simultaneous EEG and fMRI : Recording, Analysis, and Application*. 2010. ISBN: 9780199776283. DOI: 10.1093/acprof:oso/9780195372731.003.0006.

[8] R. A. Fisher. "Frequency Distribution of the Values of the Correlation Coefficient in Samples from an Indefinitely Large Population". In: *Biometrika* (1915). ISSN: 00063444. DOI: 10.2307/2331838.

[9] Lars G Hanson. "Introduction to Magnetic Resonance Imaging Techniques, Educational material." In: *Http://Www.Drcmr.Dk:8080/37* (2009).

[10] Trevor Hastie, Robert Tibshirani, and Jerome Friedman. "The Elements of Statistical Learning". In: *Elements* (2009). ISSN: 03436993. DOI: 10.1007/b94608.

[11] Emily S. Kappenman and Steven J. Luck. "The effects of electrode impedance on data quality and statistical significance in ERP recordings". In: *Psychophysiology* (2010). ISSN: 00485772. DOI: 10.1111/j.1469-8986.2010.01009.x.

[12] Pavitra Krishnaswamy et al. "Reference-free removal of EEG-fMRI ballistocardiogram artifacts with harmonic regression". In: *NeuroImage* (2016). ISSN: 10959572. DOI: 10.1016/j.neuroimage.2015.06.088.

[13] Erik K St Louis and Lauren C Frey. *Electroencephalography: An Introductory Text and Atlas of Normal and Abnormal Findings in Adults, Children, and Infants*. 2016. ISBN: 9780997975604. DOI: 10.5698/978-0-9979756-0-4.

[14] Scott Makeig et al. "Independent Component Analysis of Electroencephalographic Data". In: *Advances in Neural Information Processing Systems* (1996). ISSN: 10495258. DOI: 10.1109/ICOSP.2002.1180091. arXiv: 0310011 [q-bio.QM].

[15] Donald R. Matteson PhD Mordecai P. Blaustein MD Joseph P. Y. Kao PhD). "Cellular Physiology and Neurophysiology". In: *Mosby, Elsevier* (2012). DOI: 10.1016/C2009-0-40961-9.

[16] Maiken Nedergaard. *Garbage truck of the brain*. 2013. DOI: 10.1126/science.1240514.

[17] R. K. Niazy et al. "Removal of FMRI environment artifacts from EEG data using optimal basis sets". In: *NeuroImage* (2005). ISSN: 10538119. DOI: 10.1016/j.neuroimage.2005.06.067.

[18] Martin Olsson et al. "Sleep Deprivation and CSF Biomarkers for Alzheimer Disease". In: *Sleep* (2018). ISSN: 0161-8105. DOI: 10.1093/sleep/zsy025.

[19] Saeid Sanei and J.A. Chambers. *EEG Signal Processing*. 2007. ISBN: 9780470511923. DOI: 10.1002/9780470511923.

[20] Brendon Watson and György Buzsáki. "Sleep, memory and brain rhythms". In: *Daedalus* (2013). ISSN: 0011-5266. DOI: 10.1162/DAED.

[21] Lulu Xie et al. "Sleep drives metabolite clearance from the adult brain". In: *Science* (2013). ISSN: 10959203. DOI: 10.1126/science.1241224.

10 Appendix

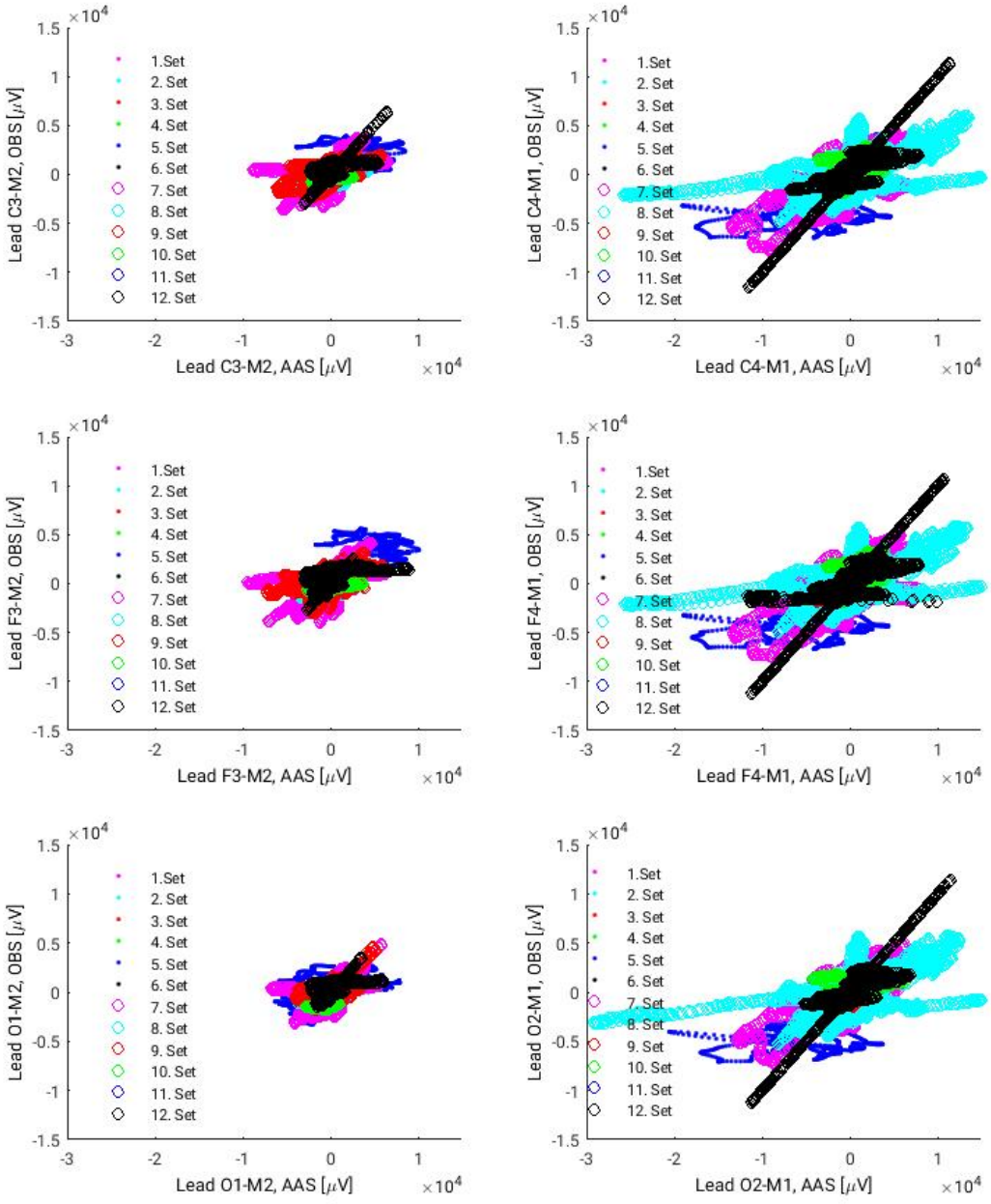

Figure 24: Scatter plot of data from lead C3-M2 (top left), C4-M1 (top right), F3-M2 (mid left), F4-M2 (mid right), O1-M2 (bottom left) and O2-M1 (bottom right), where Ballisto-cardiogram (BCG) correction has been carried out using Average Artifact Subtraction (AAS) and Optimal Basis Sets (OBS).

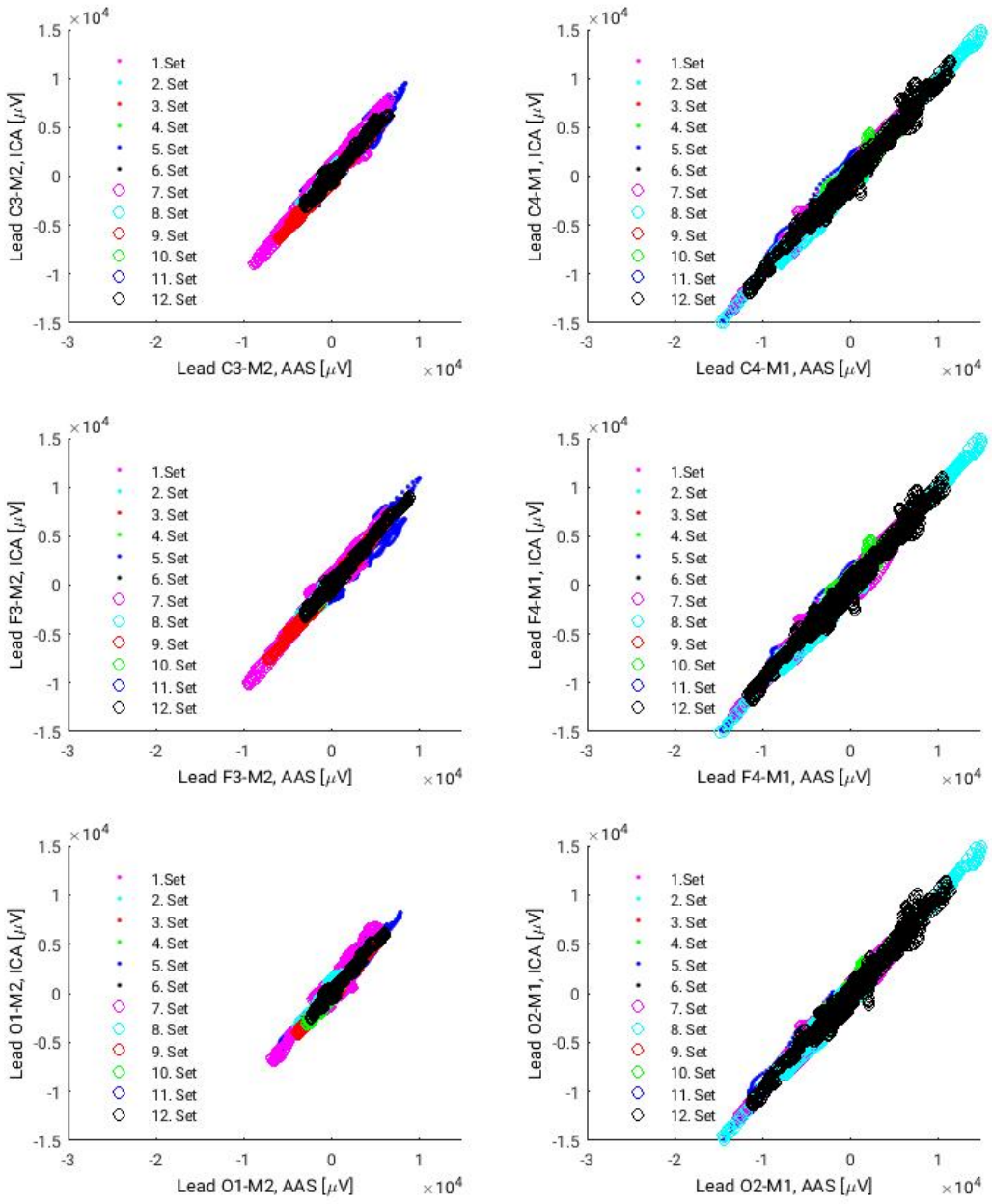

Figure 25: Scatter plot of data from lead C3-M2 (top left), C4-M1 (top right), F3-M2 (mid left), F4-M2 (mid right), O1-M2 (bottom left) and O2-M1 (bottom right), where Ballisto-cardiogram (BCG) correction has been carried out using Average Artifact Subtraction (AAS) and Independent Component Analysis (ICA).

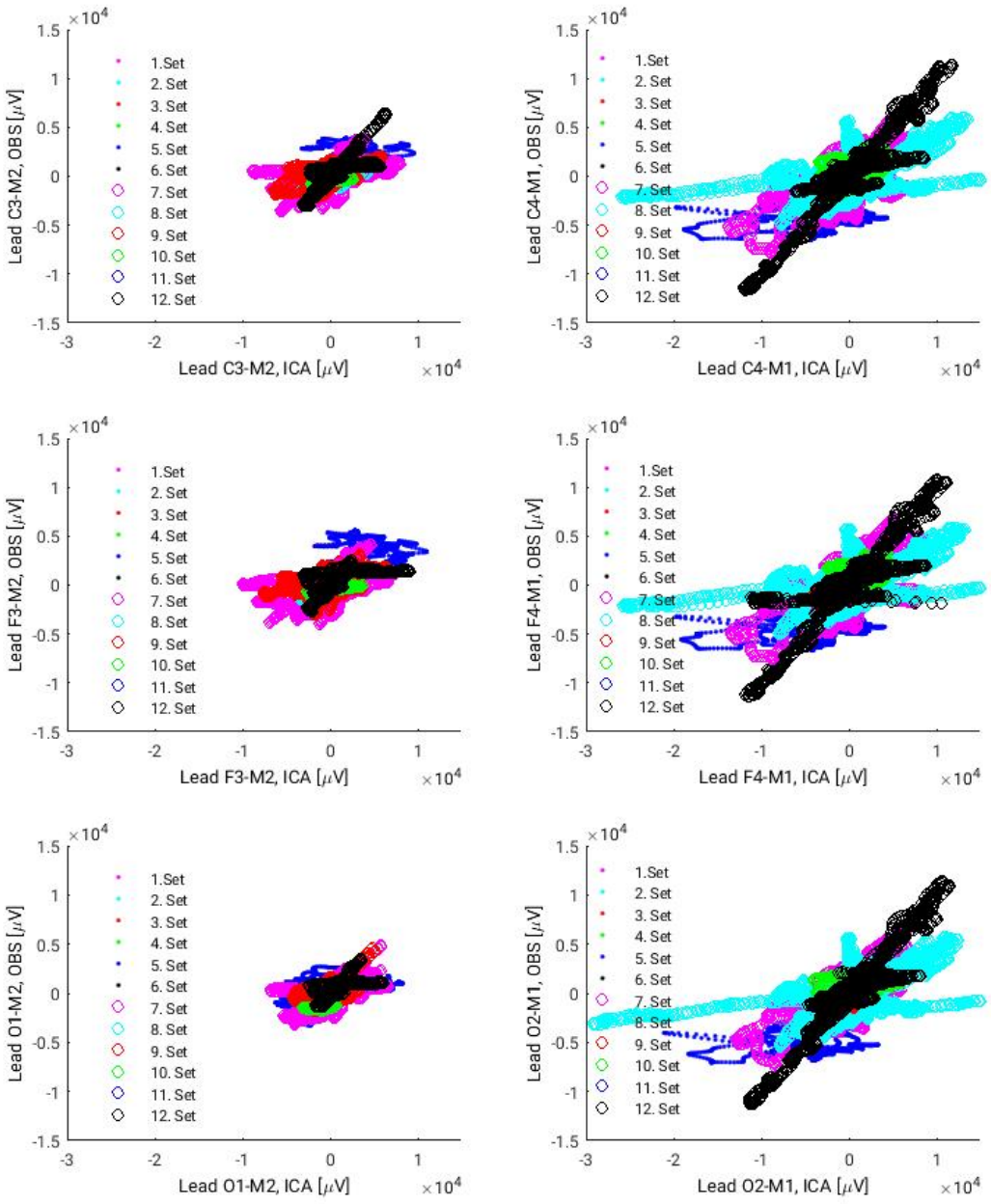

Figure 26: Scatter plot of data from lead C3-M2 (top left), C4-M1 (top right), F3-M2 (mid left), F4-M2 (mid right), O1-M2 (bottom left) and O2-M1 (bottom right), where Ballistocardiogram (BCG) correction has been carried out using Independent Component Analysis (ICA) and Optimal Basis Sets (OBS).

Lead 1	Lead 2	Mean difference	Standard deviation of difference	p-value
F3-M2	F4-M1	-0.040	0.44	0.76
F3-M2	C3-M2	0.015	0.041	0.24
F3-M2	C4-M1	-0.026	0.46	0.85
F3-M2	O1-M2	0.0047	0.12	0.90
F3-M2	O2-M2	-0.0092	0.44	0.94
F4-M1	C3-M2	-0.031	0.68	0.14
F4-M1	C4-M1	0.0091	0.037	0.41
F4-M1	O1-M2	-0.013	0.039	0.29
F4-M1	O2-M2	-0.0097	0.042	0.44
C3-M2	C4-M1	-0.036	0.071	0.11
C3-M2	O1-M2	-0.0095	0.037	0.39
C3-M2	O2-M2	-0.0076	0.029	0.38
C4-M1	O1-M2	0.035	0.076	0.14
C4-M1	O2-M2	0.028	0.30	0.75
O1-M2	O2-M2	-0.047	0.39	0.68

Table 10: Slopes of linear fit between two different leads. The mean difference between slopes of BCG correction with Average Artifact Subtraction (AAS) and Optimal Basis Sets (OBS) as well as the standard deviation and p-value are shown. An asterisk (*) denotes a significant difference.

Lead 1	Lead 2	Mean difference	Standard deviation of difference	p-value
F3-M2	F4-M1	0.011	0.058	0.52
F3-M2	C3-M2	0.0049	0.040	0.68
F3-M2	C4-M1	0.029	0.062	0.14
F3-M2	O1-M2	-0.0067	0.047	0.64
F3-M2	O2-M2	0.0097	0.058	0.57
F4-M1	C3-M2	0.014	0.037	0.22
F4-M1	C4-M1	0.0021	0.015	0.64
F4-M1	O1-M2	0.016	0.035	0.15
F4-M1	O2-M2	0.0095	0.015	0.048*
C3-M2	C4-M1	0.018	0.047	0.22
C3-M2	O1-M2	0.018	0.044	0.20
C3-M2	O2-M2	0.0074	0.013	0.066
C4-M1	O1-M2	-0.0046	0.037	0.67
C4-M1	O2-M2	0.011	0.037	0.31
O1-M2	O2-M2	0.025	0.082	0.32

Table 11: Slopes of linear fit between two different leads. The mean difference between slopes of BCG correction with Average Artifact Subtraction (AAS) and Independent Component Analysis (ICA) as well as the standard deviation and p-value are shown. An asterisk (*) denotes a significant difference.

Lead 1	Lead 2	Mean difference	Standard deviation of difference	p-value
F3-M2	F4-M1	0.051	0.44	0.70
F3-M2	C3-M2	-0.0097	0.066	0.62
F3-M2	C4-M1	0.055	0.45	0.68
F3-M2	O1-M2	-0.011	0.12	0.76
F3-M2	O2-M2	0.019	0.44	0.88
F4-M1	C3-M2	0.045	0.089	0.11
F4-M1	C4-M1	-0.0070	0.041	0.56
F4-M1	O1-M2	0.028	0.065	0.16
F4-M1	O2-M2	0.019	0.034	0.12
C3-M2	C4-M1	0.053	0.092	0.069
C3-M2	O1-M2	0.027	0.066	0.18
C3-M2	O2-M2	0.015	0.022	0.037*
C4-M1	O1-M2	-0.040	0.068	0.070
C4-M1	O2-M2	-0.017	0.31	0.85
O1-M2	O2-M2	0.072	0.42	0.57

Table 12: Slopes of linear fit between two different leads. The mean difference between slopes of BCG correction with Optimal Basis Sets (OBS) and Independent Component Analysis (ICA) as well as the standard deviation and p-value are shown. An asterisk (*) denotes a significant difference.

10.1 MATLAB scripts

In all scripts and functions in this Appendix, personal directories have been replaced by 'DIR'. Only data processing scripts have been included, not scripts for plotting. Directories are expected to contain EEGLAB, and EEGLAB must be open.

10.1.1 Function readEGI

This is the function by Pierre LeVan, Universitätsklinikum Freiburg, for loading Electrical Geodesics data.

```
function [data,fs,events] = readEGI(filename)
%READEGI reads the bin recorded using the EGI NetStation tools.
%
%   Script from Freiburg group, Pierre Levan
%
%   Edited by: Ulrich Lindberg
%   Version 1.1, June 2015

fid = fopen(filename,'r','ieee-le');

if fid==-1
    error('Could not open file');
end

```

```
header = [];
data = [];
while ~feof(fid)
    [temp_header,temp_data] = read_segment(fid);
    if isempty(header)
        header = temp_header;
    end
    % Append data at the end, but parameters should match current header
    if any(temp_header.frequency~=temp_header.frequency(1)) || ...
            temp_header.frequency(1)~=header.frequency(1)
        fclose(fid);
        error('Different sampling frequencies not supported');
    end
    if any(diff(temp_header.offsets) ~= temp_header.block_size-temp_header.offsets(end))
        fclose(fid);
        error('Different signal sizes within data block not supported');
    end
    if temp_header.ns ~= header.ns
        fclose(fid);
        error('Different number of signals in different blocks not supported');
    end
    temp_data = reshape(permute(reshape(temp_data,[],temp_header.ns,...
        size(temp_data,2)),[1 3 2]),[],temp_header.ns);
    data = [data;temp_data];
end

fclose(fid);

fs = header.frequency(1);

% Read info.xml for recording time
pathname = fileparts(filename);
xml = xmlread(fullfile(pathname,'info.xml'));
recordTime = xml.getElementsByTagName('recordTime');
recordTime = char(recordTime.item(0).getFirstChild.getTextContent);
recordTime = datenum(recordTime,'yyyy-mm-ddTHH:MM:SS.FFF');

% Read Events.xml for event times
files = dir(fullfile(pathname,'Events*.xml'));
events = struct([]);
current_index = 0;

for file_idx=1:length(files)
    xml = xmlread(fullfile(pathname,files(file_idx).name));
    xmlevents = xml.getElementsByTagName('event');
```

```
60      %Parse into a struct
61      for i=0:xmlevents.getLength-1
62          node = xmlevents.item(i).getFirstChild;
63          while ~isempty(node)
64              name = char(node.getNodeName);
65              content = char(node.getTextContent);
66              if ~strncmp(name,'#',1)
67                  events(current_index+1).(name) = content;
68              end
69              node = node.getNextSibling;
70          end
71          current_index = current_index+1;
72      end
73  end
74
75  for i=1:length(events)
76      events(i).beginTime = (datenum(events(i).beginTime,'yyyy-mm-ddTHH:MM:SS.FFF')...
77          -recordTime)*86400;
78  end
79
80  function [header,data] = read_segment(fid)
81
82  current_offset = ftell(fid);
83
84  header.version = fread(fid,1,'uint32');
85
86  if header.version~=1
87      fclose(fid);
88      error('Version ~= 1');
89  end
90
91  header.header_size = fread(fid,1,'uint32');
92  header.block_size = fread(fid,1,'uint32');
93  header.ns = fread(fid,1,'uint32');
94  header.offsets = fread(fid,header.ns,'uint32');
95
96  depth_frequency = fread(fid,header.ns,'uint32');
97  header.depth = bitand(depth_frequency,255,'uint32');
98  header.frequency = bitshift(depth_frequency,-8,'uint32');
99  if any(header.depth~=32)
100     fclose(fid);
101     error('Currently only 32-bit data supported');
102 end
103
104 header.hl = fread(fid,1,'uint32');
```

```
header.optional_header = fread(fid,header.hl/4,'uint32');

% Start reading until the header changes
fseek(fid,header.block_size,'cof');
header_flag = fread(fid,inf,'uint32',header.block_size);

n_blocks = find(header_flag,1);
if isempty(n_blocks)
    n_blocks = length(header_flag)+1;
end

fseek(fid,current_offset+header.header_size,'bof');
data = fread(fid,[header.block_size/4 n_blocks],sprintf('%d*float32',...
    header.block_size/4),4);

if ~feof(fid)
    fseek(fid,-4,'cof');
end
```

10.1.2 Script for cutting data sets

```
%% Script for cutting EEG data according to fMRI-sequences
%%%%% By Anders Olsen


%% Locate files

INPFILE=(DIR)

%%
    for i=3%:length(INPFILE)
    [path,file] = fileparts(INPFILE{i});
    path_split=strsplit(INPFILE{i},'/');

    %specify new path
    newpath=fullfile('DIR');

    %Specify new file name.
    newfilename=strcat(newpath,path_split(6),path_split(7));

    % Read the EGI data and events using readEGI
    [EEGdata,fs,events] = readEGI(fullfile(INPFILE{i},'signal1.bin'));

    % Load ECG data
    ECGdata = readEGI(fullfile(INPFILE{i},'signal2.bin'));

```

```
% Choose channels if you only want to process parts of the EEG-data
% remember these for when plotting.
% In the data processing sections these will be named 1 and onwards
%chosenchans=channels;
I=1:256;
% Concatenate EEG and ECG data
data = [EEGdata(:,I) ECGdata]';
chanlabels = struct('labels',[strcat('E',cellstr(num2str((1:length(I))','%-d'))); 'ECG']


% EEG lab - create dataset

EEG = pop_importdata('setname',INPFILE{i},'data',data,'dataformat','array','srate',fs,'c
EEG = eeg_checkset(EEG);
EEG.nbchan=size(EEG.data,1); EEG.ECGch=EEG.nbchan;
%EEG.data=double(EEG.data'-mean(EEG.data'))';
EEG.rawdata=EEG.data; % If we want to save raw data

% Calculate datapoints at which trigger signals are located

Trigger=fix([events(strcmp('TREV',{events.code})).beginTime]*EEG.srate);


%% cut data set

Triggerdiff=diff(Trigger); %Utilize high distance between triggers
newTrigstart=Trigger(1);
for k=1:length(Triggerdiff)
    if Triggerdiff(k)>1000
        newTrigstart(k+1)=Trigger(k+1);
        k1=k;
        oldTrigend(k)=Trigger(k);
    end
end
oldTrigend(length(Triggerdiff)+1)=Trigger(end);
oldTrigend(oldTrigend==0)=[];
newTrigstart(newTrigstart==0)=[];
% Remember to clear vars later
%%
EEGtemp=EEG;
if length(newTrigstart)==1
    EEGtemp.data=EEGtemp.data(:,newTrigstart(1)-EEGtemp.srate:oldTrigend(1)+EEGtemp.srat
    EEGtemp.Trigger=Trigger;
    EEGtemp.Trigger=EEGtemp.Trigger-EEGtemp.Trigger(1)+EEGtemp.srate;
    EEG1file=strcat(newpath,'pilot0MREG',num2str(i));
```

```
        EEG=EEGtemp;
        save(EEG1file,'EEG')
        %pop_saveset(EEG,'filename',[EEG1file{1},'.set']);
    end

    if length(newTrigstart)==2
        EEG1=EEGtemp;
        EEG1.data=EEG1.data(:,newTrigstart(1)-EEG1.srate:oldTrigend(1)+EEG1.srate);
        EEG1.Trigger=Trigger;
        EEG1.Trigger(EEG1.Trigger>=oldTrigend(1)+1000)=[];
        EEG1.Trigger=EEG1.Trigger-EEG1.Trigger(1)+EEG.srate;
        EEG1file=strcat(newfilename,'MREG');
        EEG=EEG1;
        save(EEG1file{1},'EEG')
        %pop_saveset(EEG,'filename',[EEG1file{1},'.set']);

        EEG2=EEGtemp;EEG2.data=EEG2.data(:,newTrigstart(2)-EEG2.srate:oldTrigend(2)+EEG2.sra
        EEG2.Trigger=Trigger;
        EEG2.Trigger(EEG2.Trigger<=newTrigstart(2)-EEG.srate)=[];
        EEG2.Trigger=EEG2.Trigger-EEG2.Trigger(1)+EEG.srate;
        EEG2file=strcat(newfilename,'MB');
        EEG=EEG2;
        %pop_saveset(EEGMULTI,'filename',[EEG2file{1},'.set']);
        save(EEG2file{1},'EEG')
    end

    clearvars newTrigstart oldTrigend
end
```

10.1.3 Function for performing AAS, OBS and ICA

```
% By Anders Olsen
% To run artifact removal on EEG-data recorded during a single MRI sequence
% The script runs 3 different methods:
%-  Average artifact subtraction (Allen et al., 2000) for Gradient artifact
%   and ballistocardiogram removal
%-  Optimal Basis Sets (Niazy et al., 2005) for Gradient artifact and
%   ballistocardiogram removal
%-  Independent Component Analysis (Makeig et al., 1997) for
%   ballistocardiogram removal
%
% The output is an eeglab structure named EEG
% This structure contains the following data:
%
%   Raw data: EEG.rawdata
%   gradient removal with aas
```

```
%   gradient removal with OBS
%   Gradient removal with aas and BCG removal with aas: EEG.GA_aas_BCG_aas
%   Gradient removal with aas and BCG removal with obs: EEG.GA_aas_BCG_obs
%   Gradient removal with aas and ICA variables



newpath=fullfile('DIR');
FILESMB=dir(['DIR']);
FILESMREG=dir(['DIR']);
for i=6:size(FILESMB,1)
    %% Load data and convert to double precision
    tic
    load(strcat(FILESMB(i).folder,'/',FILESMB(i).name));
    EEG.ECGch=size(EEG.data,1);
    EEG.data=double(EEG.data);
    newfilename=strcat(newpath,'MB',string(i)); %New file be saved as

    %% Gradient correction


    EEGtemp = fmrib_fastr(EEG,70,20,30,EEG.Trigger,1,0,0,[],[],0.03,[],0);
    EEG.GA_aas = EEGtemp.data;
    EEGtemp=fmrib_fastr(EEG,70,20,30,EEG.Trigger,1,0,0);
    EEG.GA_obs=EEGtemp.data;


    %%%%%%%%%%%%%%%%%%%%%%%%
    %% Fixing after Gradient correction: demeaning and removal of first and last second
    EEG.GA_aas(:,1:2000)=[];
    EEG.GA_aas(:,end-2000:end)=[];
    EEG.GA_aas=EEG.GA_aas-mean(EEG.GA_aas,2);
    EEG.GA_obs(:,1:2000)=[];
    EEG.GA_obs(:,end-2000:end)=[];
    EEG.GA_obs=EEG.GA_obs-mean(EEG.GA_obs,2);

    %% QRS detection with adaptive thresholding (Niazy et al., 2005)
    %  and subsequent BCG removal with aas and obs
    %  ECG channel is high-pass filtered to ensure correct QRS detection

    % QRS detection
    EEGtemp=EEG;
    EEGtemp.data=double(EEG.GA_aas);
    EEGtemp.ECGft=fftshift(fft(EEGtemp.data(EEGtemp.ECGch,:)'));
    EEGtempfreq=linspace(-EEG.srate/2,EEG.srate/2-EEG.srate/length(EEGtemp.ECGft),length(EEG
```

```
    EEGtemp.ECGft(abs(EEGtempfreq)<=0.5)=0; %Set some frequencies to zero
    EEGtemp.data(EEGtemp.ECGch,:)=real(ifft(ifftshift(EEGtemp.ECGft)));

    EEG.QRS_GA_aas = fmrib_qrsdetect(EEGtemp,EEGtemp.ECGch); %run algorithm
    EEG.QRS_GA_aas_fordet=EEGtemp.data(EEGtemp.ECGch,:);



    EEGtemp=EEG;
    EEGtemp.data=EEG.GA_aas;
    EEGtemp = fmrib_pas(EEGtemp,EEG.QRS_GA_aas,'obs',4);
    EEG.GA_aas_BCG_obs=EEGtemp.data;

    EEGtemp.data=EEG.GA_aas;
    EEGtemp = fmrib_pas(EEGtemp,EEG.QRS_GA_aas,'mean');
    EEG.GA_aas_BCG_aas=EEGtemp.data;

    %% ICA

    EEGtemp=EEG;
    EEGtemp.data=EEG.GA_aas(1:256,:); %Without ECG channel

    EEGtemp=pop_editset(EEGtemp,'pnts',[1]); %set amount of frames
    EEGtemp = pop_runica(EEGtemp,'icatype','runica','chanind',1:256,'extended',1);
    EEG.GA_aas_BCG_ica=EEGtemp.data;
    EEG.GA_aas_BCG_icawinv=EEGtemp.icawinv;
    EEG.GA_aas_BCG_icasphere=EEGtemp.icasphere;
    EEG.GA_aas_BCG_icaweights=EEGtemp.icaweights;
    EEG.GA_aas_BCG_icachansind=EEGtemp.icachansind;


        %% save the struct
    save(newfilename,'EEG','-v7.3')
end
```

10.1.4 Script for removing ICA components automatically

```
%%% By Anders Olsen
%% Average artifacts in independent components

FILES=dir(['DIR']);
clearvars -except FILES
newpath=fullfile('DIR');

for i=1:12
    clearvars -except FILES i newpath
```

```
10      load(strcat(FILES(i).folder,'/',FILES(i).name));
11          newfilename=strcat(newpath,string(i)); %New file be saved as
12
13
14      EEG2=EEG;
15      EEG2.data=EEG.GA_aas;
16      EEG2.icaweights=EEG.GA_aas_BCG_icaweights;
17      EEG2.icasphere=EEG.GA_aas_BCG_icasphere;
18      EEG2.icawinv=EEG.GA_aas_BCG_icawinv;
19      EEG2.icachansind=EEG.GA_aas_BCG_icachansind;
20      EEG2=pop_editset(EEG2,'pnts',[1]);
21
22      tmpdata1 = eeg_getdatact(EEG2, 'component', [1:size(EEG2.GA_aas_BCG_icaweights,1)]);
23
24
25      spb=round(mean(diff(EEG.QRS_GA_aas))); %samples per beat
26      for k=1:size(tmpdata1,1)
27          avg(k,:)=tmpdata1(k,EEG.QRS_GA_aas(1):EEG.QRS_GA_aas(1)+spb-1);
28          for i=2:length(EEG.QRS_GA_aas)-1
29              avg(k,:)=avg(k,:)+tmpdata1(k,EEG.QRS_GA_aas(i):EEG.QRS_GA_aas(i)+spb-1);
30          end
31          avg(k,:)=avg(k,:)/(length(EEG.QRS_GA_aas)-1);
32          % triangle(EEG.QRS_GA_aas(i)-50:EEG.QRS_GA_aas(i)+50)=x;
33      end
34
35      %%% Construct new component signal
36      artisign=zeros(size(tmpdata1,1),size(tmpdata1,2));
37      for k=1:size(tmpdata1,1)
38          for i=1:length(EEG.QRS_GA_aas)
39              artisign(k,EEG.QRS_GA_aas(i):EEG.QRS_GA_aas(i)+spb-1)=avg(k,:);
40          end
41      end
42      artisign=artisign(1:size(tmpdata1,1),1:size(tmpdata1,2));
43
44      %%% Corrcoef with avg artifact
45      for i=1:size(EEG2.icaweights,1)
46          [r,p]=corrcoef(artisign(i,:),detrend(tmpdata1(i,:),'constant'));
47          r3(i)=r(1,2)*r(1,2);
48          p3(i)=p(1,2);
49      end
50      [~,I4]=sort(r3,'descend')
51      r4=r3>0.05;r4(r4==0)=[];
52      comps=1:256;
53      remove=I4(1:length(r4));
54
```

```
55      EEG2=pop_subcomp(EEG2,sort(remove));
56      EEG.GA_aas_BCG_ica=EEG2.data;
57      save(newfilename,'EEG','-v7.3')
58
59
60  end
```